Public document

Field measurements realized on selected test sites

FP7 – DIGISOIL Project Deliverable D3.2

N° FP7-DIGISOIL-D3.2
December 2010

The DIGISOIL project (FP7-ENV-2007-1 N°211523) is financed by the European Commission under the 7th Framework Programme for Research and Technological Development, Area "Environment", Activity 6.3 "Environmental Technologies".

Geoscience for a sustainable Earth

Public document

Field measurements realized on selected test sites

FP7 – DIGISOIL Project Deliverable D3.2

N° FP7-DIGISOIL-D3.2
December 2010

G.Grandjean (BRGM)
With the collaboration of
R. Maftei (GIR), M. Séger (INRA), I. Cousin (INRA), G. Giot (INRA), G.Coulouma (INRA), A. Besson (INRA), F. André (FZJ), S. Lambot (FZJ), J. Thiesson (INRA), F. Garfagnoli (UNIFI), S. Moretti (UNIFI), A. Steevens (UCL), B van Wesemael (UCL), M Nocita (UCL), K. Samyn (BRGM)

Checked by:	**Approved by**:
Name: B. van Wesemael	Name: G.Grandjean
Date: 06/03/10	Date: 06/03/10
☑	☑

BRGM's quality management system is certified ISO 9001:2000 by AFAQ.

The DIGISOIL project (FP7-ENV-2007-1 N°211523) is financed by the European Commission under the 7th Framework Programme for Research and Technological Development, Area "Environment", Activity 6.3 "Environmental Technologies".

Geoscience for a sustainable Earth
brgm

Keywords: geophysics, soil properties, field experiments, laboratory experiments, calibration, controlled conditions

In bibliography, this report should be cited as follows:
G.Grandjean, R. Maftei, M. Séger, I. Cousin, G. Giot, G.Coulouma, A. Besson, F. André, S. Lambot, J. Thiesson, F. Garfagnoli, S. Moretti, A. Steevens, B. van Wesemael, M. Nocita, K. Samyn, 2010. Field measurements realized on selected test sites. Report N°BRGM/FP7-DIGISOIL-D3.2; 84 pages.

Synopsis

This deliverable D3.2 (Site preparation) is linked to the first task (3.1) of DIGISOIL's WP3 (Implementation, field testing and validation on selected test sites). The objectives are here to report all the experiments that have been conducted on real test sites to evaluate the proposed methodology. Test sites are identified as Luxembourg (LU), Mugello (IT) and Zala (HU). For each geophysical method, the experimental conditions, data acquisitions, validation points and produced maps are presented.

The optimal combination of petrophysical parameters are used to describe the aforementioned soil properties. The inference functions and fusion techniques developed in WP 2 are applied to the field conditions of the different test sites. Where possible geo-referenced data sets and maps were used for calibration and validation of the geophysical techniques. In some cases, additional analyses can be required to fill the gaps in the datasets and cover the selected dynamic soil properties. The experimental conditions, the results and the costs of the experiments and measurements for each geophysical method (Hyperspectral, GPR, EMI, Geoelectric, Seismic), in terms of man-day, are reported.

After a general introduction that indicates the specific content of this deliverable in relationship with the deliverables of WP2 and other deliverables of WP3, each experiment is described in detail. The plan is organized by experimentations but several geophysical methods may have been run at the same site.

Contents

List of illustrations

List of tables

1. Introduction

As mentioned in the WP2 deliverables, the main objectives of the experimentations are to demonstrate the feasibility of retrieving soil characteristics from geophysical measurements. In this deliverable, we will specifically focus on the measurements of geophysical parameters and the soil characteristics (Figure 1), respectively used in map production and calibration. We remind here that the soil characteristics of interest are the carbon content, the clay content, the water content, and the bulk density or soil stiffness. As all these soil characteristics may change with depth due to soil horizonation, a fundamental ancillary data associated with all these soil characteristics is the soil depth.

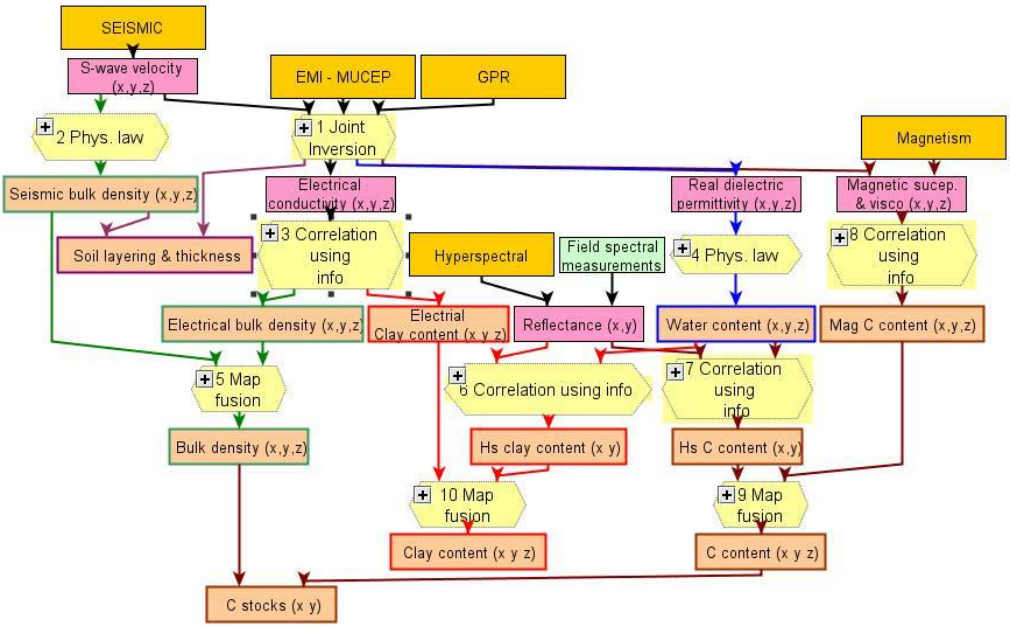

Figure 1: General scheme of the DIGISOIL project to link geophysical measurements to soil characteristics. The red line limits the content of this deliverable, that intends to link geophysical parameters (pink) to soil characteristics (brown).

In the Figure 1, the relationships between geophysical parameters and soil characteristics are represented by arrows. The objective of this deliverable is not to discuss the nature of the arrows, say the processing tools that will be used to link the geophysical parameters to the soil characteristics. This point has been discussed in the D2.2 report. We only report here experiments linking geophysical parameters and soil characteristics.

The following sections describe the geophysical experiments conducted on selected test sites, Mugello (Italy), Louxembourg, Zala (Hungary; Figure 2) in order to link geophysical parameters to soil characteristics. Each paragraph corresponds to a geophysical method, and can be associated to one or more soil parameters. In some cases, several geophysical methods have been used during the same experiment, but the experiment is of course described only once.

Figure 2 : Validating test sites

- LUXEMBOURG (LU)

The pilot zone consists of a number of cropland fields (c. 30) along a transect in the Grand Duchy of Luxembourg to cover a wide range of parent materials, soil types, SOC content and ranging from extensive livestock farms to arable farms with low manure input. Although of a small extent (2586 km2), Luxembourg is characterized by a very diverse physiogeography. Five distinct agrogeopedological zones can be distinguished: (1) the Oesling in the north covering one third of the country is a homogeneous schist Hercynian massif with a mean altitude of 450 m. Main soil texture is sand and loam. The southern part of Luxembourg, called the Gutland, covers two thirds of the country. In this area, four different agro-geopedological zones are distinguished: (2) the Minette basin in the south is characterized by red loamy/clay soils, formed by marls and sandstones covered with ferrous sediments; (3) the Moselle region characterized by Keuper and limestone with clay and lime soil types; (4) central part of the Gutland in the Luxembourgish sandstone area with sandy soils; (5) the Rédange-Diekirch area with soils of the loam-loess type on red sandstone and Luxembourgish sandstone. In the southern part of Luxembourg (Gutland), the most common crop rotation is a three years rotation with winter wheat, winter barley and silage maize. The field on which all geophysical experiments were carried out is in the Northern part of Luxembourg (Oesling). The field of 5 ha is slightly sloping to the West starting on a plateau. Soils are generally thin and

stony. A detailed description of three soil profiles and a soil map of the field are given in section 2.1.

- MUGELLO (IT)

In Central Tuscany, and more particularly, in the hillsides north of Florence, soils with agricultural suitability have a high economic value mainly connected with the production of internationally famous wines and olive oils. Sediment yield and consequently soil losses are produced by two different mechanisms, erosion and landsliding, which affect all the types of land use. Even small disturbances induce potential economic losses which must be considered in farming management practices. The test area is formed by a number of fields located in the Mugello basin, located about 30 km north of Firenze and it is extended for about 20 km^2.The geological terrains outcropping in these zones are fluvio-lacustrine deposits, ranging in age between lower Pliocene and Upper Pleistocene, forming low-dipping lenticular beds. From the pedological point of view, more or less eroded soils prevail (utric and calcareous Regosols and lytic Leptosols), soils with pedogenetic structure at depth and weakly differentiated profiles (eutric and calcareous Cambisols), soils with clay masses (gleich Luvisols), acidic soils with accumulation of organic material (humic Umbrisols) and anthropically terraced soils (anthropic Regosols). Agriculturally suitable terrains are assigned mainly to annual crops, marginally to olive groves, vineyards and orchards. Climate is temperate-hot, with cold winters and mildly hot to hot summers and medium to intense rainfalls, concentrated in the autumnal months.

- ZALA (HU)

The pilot area is situated in Zala County in the western Hungary. The centre of the pilot area has the following coordinates: Latitude: 46°50'0.99"N, Longitude: 17° 6'14.68"E. The whole area is 744 km2 large. From the whole pilot area (744km2) are available DEM (5x5 m GRID), topographical maps with 0,875m/pixel accuracy, ortophotos with 0,5m/pixel accuracy and cadastral maps to represent ownerships. There are available 1:10 000 scale soil maps from about 20 000 ha. Large scale soil maps consist of several cartograms to represent the soil information. The base layer shows the soil subtype, the parent material and the texture of the upper tilled layer. The other layers of soil data represent the remaining soil information, like humus, pH and lime content, ground water and salinization properties. Soil profile data is also available from about 10 000 ha large area which contains all the soil information of all soil profiles from all horizons. The soil profile database contains information on the following items: horizon depth, soil subtype, texture, parent material, pH, humus, salt, lime content. The selected agricultural area within the pilot area is 2845 ha large (43 registered parcels) where there are available long-term yield data and soil test data, too. Soil test data from three different years are available from all of the parcels.

The following table gives an overview of the experimentations realized on test sites.

Localization *Site coordinator*	**Soil properties to be investigated**	**Techniques applied on the sites**	**Site characteristics**	**Associated Soil types (WRB)**	**Obtained results**
Luxembourg-LU *UCL*	C content Density/Stifness Hydro. Prop. Soil depth	Hyperspectral Magnetism Geoelectric/EM GPR	Southern Belgium/Luxembourg: atlantic area Intensive agriculture Airborne & field data available	UMBRISOL (Hyperdistric) CAMBISOLS ANTHROSOL	C content map Soil depth map Water content map Clay content map Stone content
Mugello-IT *UNIFI*	C content Soil depth Clay content	Hyperspectral Seismic GPR/EM Geoeleftric	Mediterranean area Traditional agriculture Soil database availlable (OM, erosion model)	Calcaric REGOSOL	C content map Soil depth map Water content map Clay content map
Zala-HU *UPA*	Water content	Geoelectric	Western Hungary: continental area Intensive & traditional agriculture	Haplic CAMBISOL, Haplic LUVISOL (majority), arenic LUVISOL, FLUVISOL	Water variability on time

Tableau 1 : Test sites and their characteristics (Area's typologies are from the "Indicative map of the European biogeographical regions", 2005).

2. Luxembourg site

2.1. SITE LOCALISATION AND PRESENTATION OF THE STUDIED AREA

- Pedologic description

This parcel is situated in the Oësling hills in the north part of the Grand Duchy of Luxembourg with a mean altitude of 450 m. The soils were developed on schist materials partly intricated within phyllites. Three soil pits were dug in order to descibe and analyse soil characteristics. The spatial pattern of soils in this parcel was described with 50 additionnal auger holes. Three main soil units were found and delimited (Figure 3).

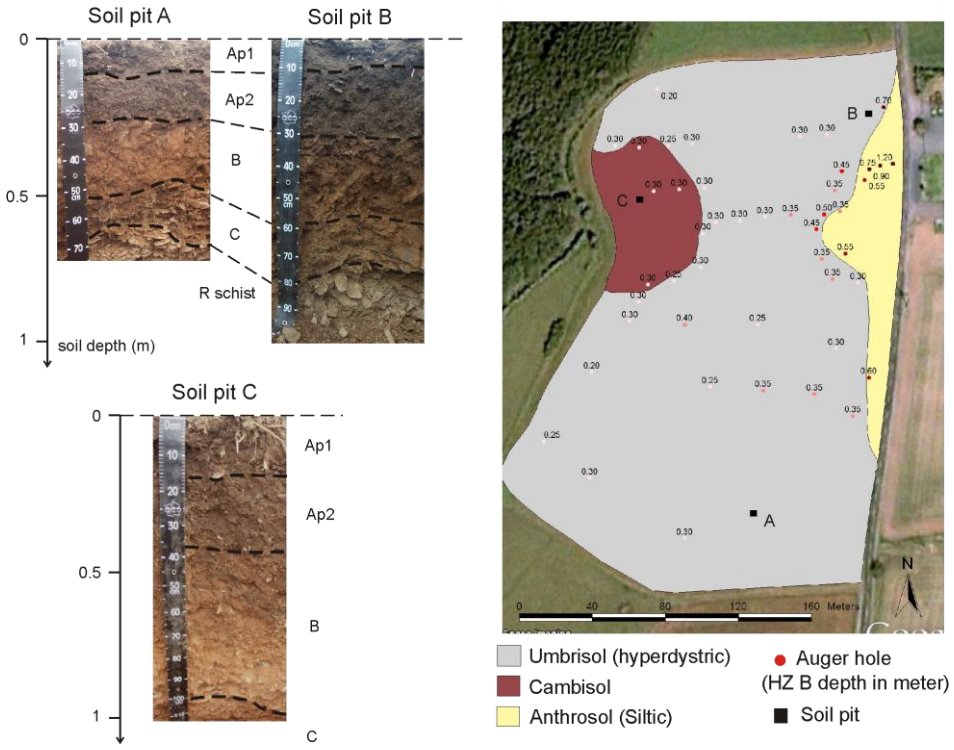

Figure 3 : Pedologic desciption of the studied area. The value associated with dot is the depth of the B horizon.

Soil unit 1 constitutes the main soil unit of the block, characterised by the soil pits A and B. The tilled layer (Ap) is organic, dark browny, with a medium texture (sandy clay loam) and a granular structure, and contains about 15-20% of schist

fragments. The pedogenetic horizon (B) is a brown clay loam with a angular blocky structure and contains more than 30 % of schist fragments. The rock fragments content is higher in the C horizon.

Soil unit 2 corresponds to an accumulation in the bottom part of the parcel due to past erosion. The soil depth is higher than the depth of the soil unit 1. The B horizon is more reddish because of preferential water circulation in the bottom part of the parcel. The C horizon appears at 0.9 meter depth.

Soil unit 3 has developed alongside the road and was strongly affected by human activities, probably at the period of the road construction. The layers within the first 0.6 meters are silty, with a massive structure and without any rock fragments. These layers overlay a A horizon similar to the A horizon described in the soil unit 1.

The depth of the B horizon is relatively constant, around 30 cm.

An analysis of the soil structure within the tilled layers is realised using a morphological description (Figure 4) in pit A. This technique aims at describing the different elements in the macrostructure (compacted clods, porous media, cracks).

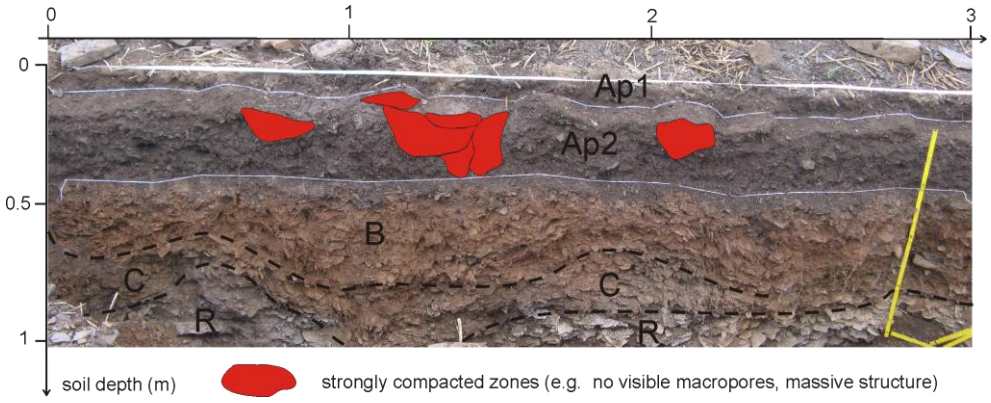

Figure 4 : Morphological profile, dig perpendicularly to the main tillage direction pit A)

Strongly compacted zones were identified thanks to their specific features, i.e. no visible macropores, massive structure and smooth breaking surfaces. The figure shows very few proportion of such compacted zones within the tilled layers, (except at the 1,2 meter location from the left border of the picture). This compacted zone is probably due to tractor wheeling at the time of previous works before the last superficial tillage.

These observations can be extrapolated to the whole part of the parcel, where the same tillage operations have been conducted. However, the structure may be modified in the South part of the plot due to an increase of soil moisture content at the time of the tillage operations. This is consistent with the bulk density results that show higher values in the South part of the plot than at the North.

- Topographic map with sampling locations

A topographic map was realised by a precise DGPS installed in the ARP system. As shown in Figure 5, the studied area exhibits high change in altitude, with 10 meters differences between the highest and the lowest points. A talweg is located in the middle of the parcel, in the West-East direction.

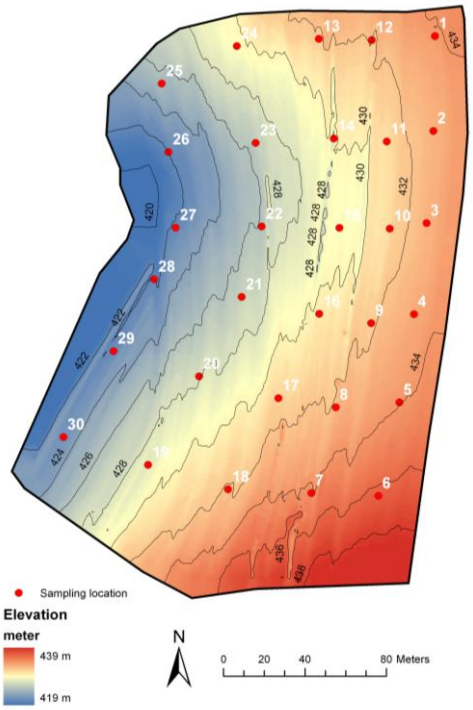

Figure 5 : Topographic map and locations of soil sampling

Thirty soil cores were sampled in a regular grid in the studied area for the validation. The cores were taken using a percussion hammer and a 9.5 cm cylinder until a depth at which the stone content hampered a further penetration into the soil (less than 60 cm; Figure 6).

The cores were cut into 10 cm slices and sealed in plastic bags. The moisture content, stone content, bulk density, C content (Variomax CN analyser) and soil texture (Coulter counter) were determined in the laboratory. The compaction of the soil cores was minimal as indicated by comparing the length of the soil core with the depth of the hole. Overall the moisture content was somewhat higher in the topsoil, the C content decreased with depth, while the stone content and bulk density increased with depth (Figure 7).

Figure 6 : Sampling of the soil cores for validation

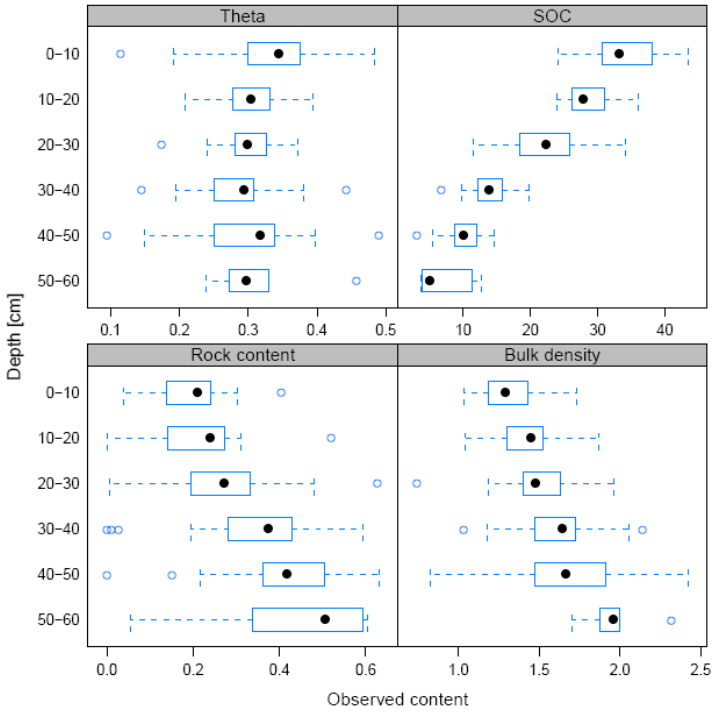

Figure 7 : Box and whisker plots of the soil properties in the validation cores and their depth distribution.

- C content

The soil organic carbon content decreases with depth (Figure 8). For some points, the soils were too stony to sample the 30-40 cm layer, and values of 0 g C kg^{-1} are given on the maps.

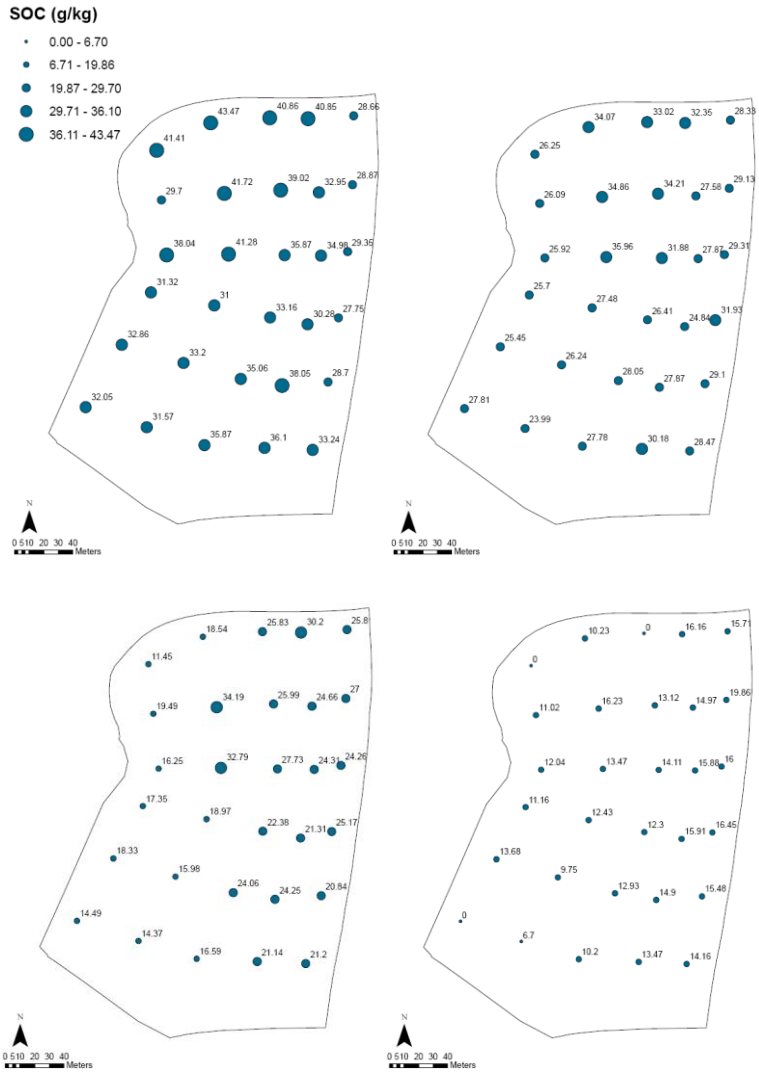

Figure 8 : SOC content of the 0-10 cm layer (upper left panel), 10-20 cm (upper right panel), 20-30 cm (lower left panel) and 30-40 cm (lower right panel)

- Clay content

The clay content was determined in the plough layer (0-10 cm) and just below the plough layer (20-30 cm).

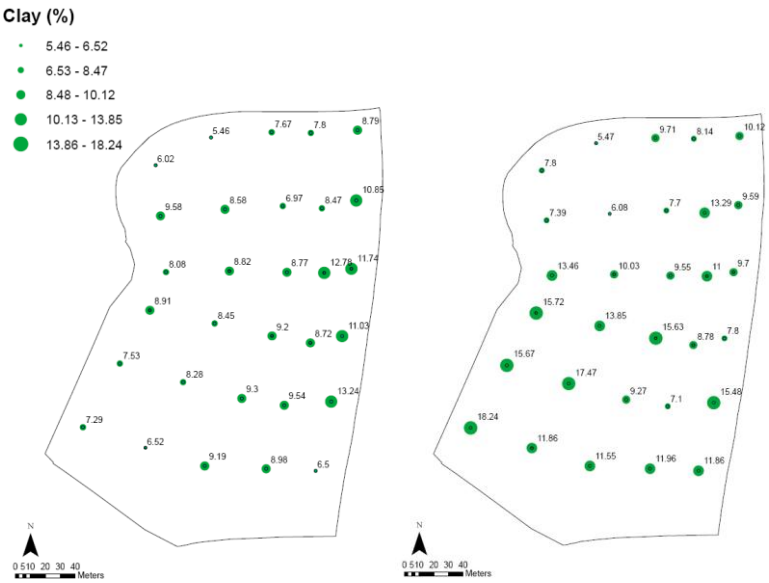

Figure 9 : Clay content for the 0-10 cm layer (left panel) and 20-30 cm layer (right panel)

- Water content

TDR values are not presented here because the high stone content over the whole studied area did not allow correct measurements with this method. The volume water content was measured directly in the fine earth from the soil cores. It does not reflect the real water content in the horizon, because the hydric properties of the stones are here not taken into account.

The water content in the surface horizon is high (values usually larger than 0.25 g.g-1), due to a rain event the day before the measurements. From 0 to 30 cm, the water content is higher in the central part of the studied area, in the thalweg zone. Higher values are observed in the anthropogenic North-East part. In the deeper horizons, the spatial organization of the water content is different and does not seem to be related to any surface topography.

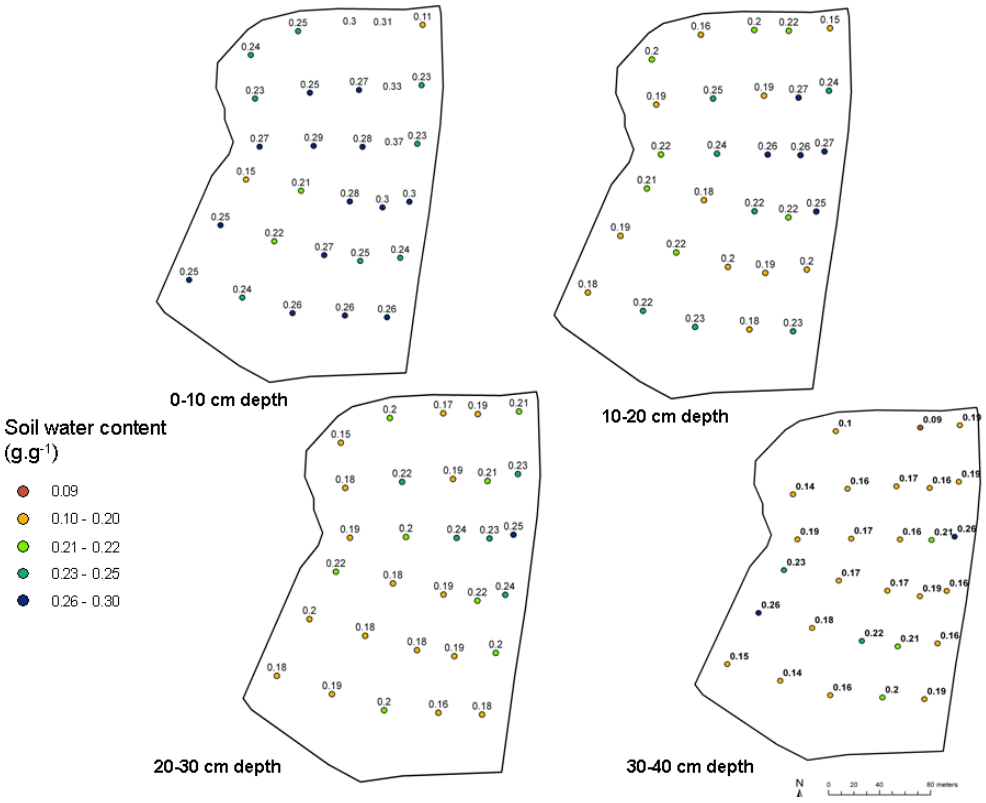

Figure 10 : Spatial distribution of the gravimetric water content

- Rock content

The rock content is estimated from driller samples analysis. Figure 11 shows the spatial distribution of rock content at 4 depths.

According to the Soil Survey Staff (2003), soils can be considered as stony soils when the volume rock content exceeds 35 %. In that case, the soil physical properties can be strongly affected by stones. In the studied parcel, stones are present even in the surface horizon, especially in the North-West part. In the deepest horizon (30-40 cm), stone content is usually higher than 30 %.

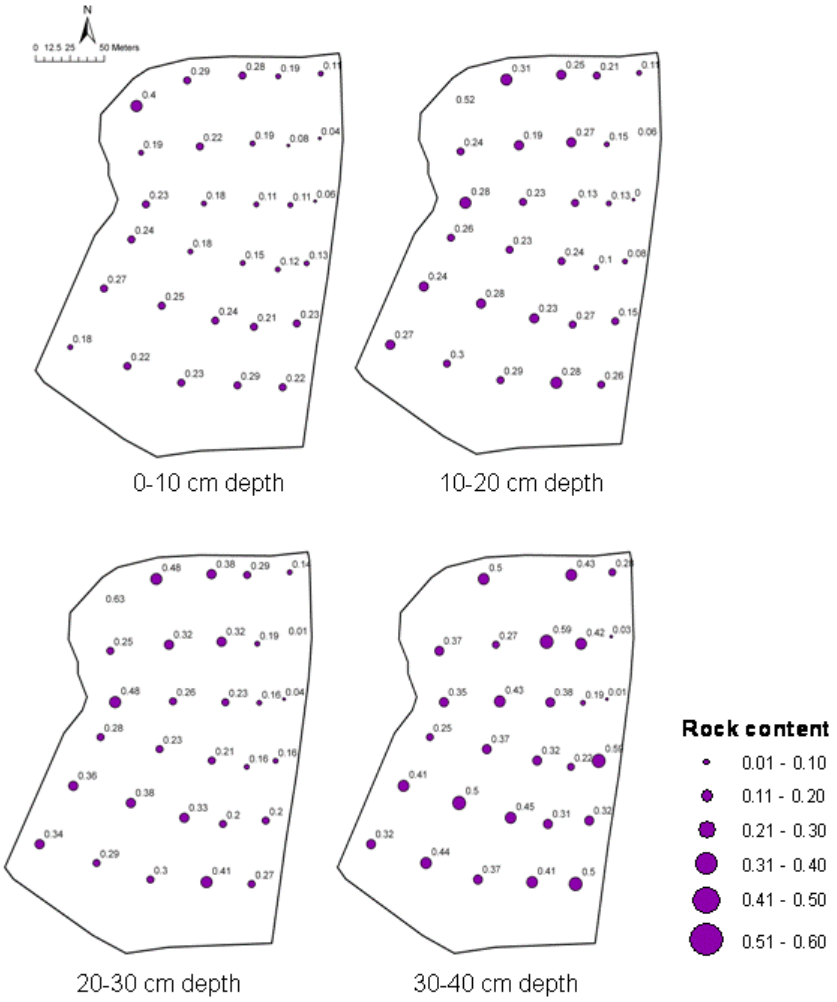

Figure 11 : Spatial distribution of the rock volume content

- Bulk density map

The bulk density has been measured on the soil cylinders. This value includes the effect of stones, the bulk density of the fine earth and the macroporosity. To interpret data, additional measurements have shown that i) the solid bulk density in the stones, measured by a gas pycnometer is equal to 2.7 $g.cm^{-3}$, and ii) the apparent bulk density measured by Archimede's method using kerosene is equal to 2.7$g.cm^{-3}$.

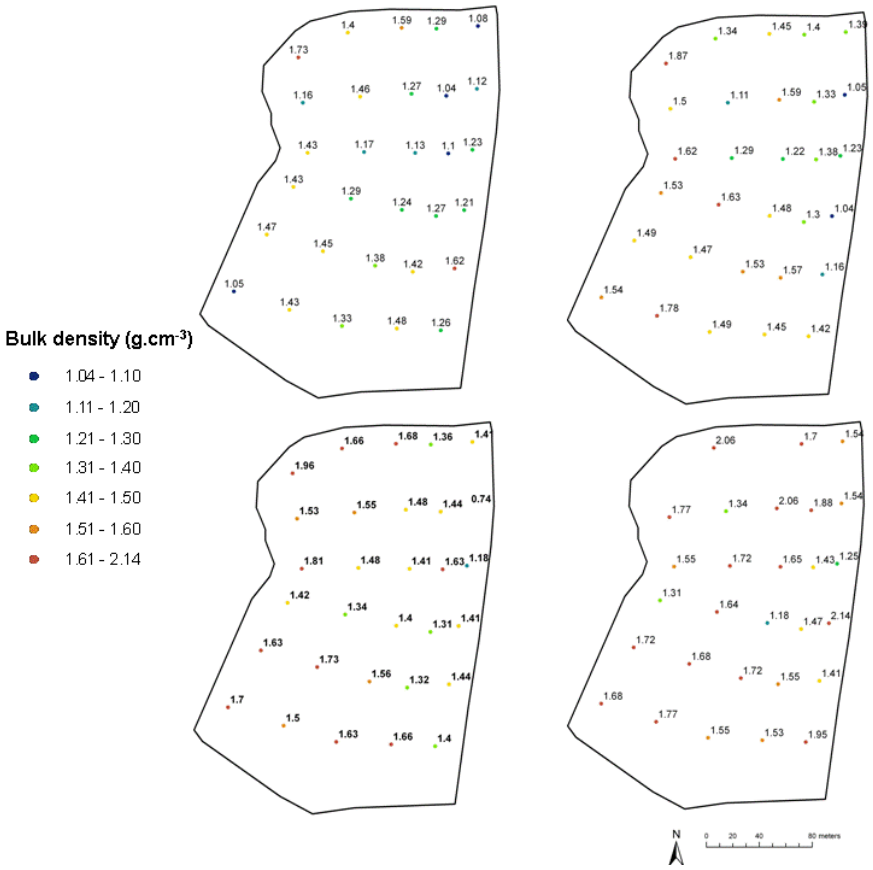

Figure 12 : Bulk density maps

As seen on the Figure 12, the bulk density is highly variable. It can sometimes reach values higher than 2 $g.cm^{-3}$, or values lower than 1.1 $g.cm^{-3}$. As a comparison, usual bulk density values in cultivated soils are comprised between 1.3 $g.cm^{-3}$ for porous horizons and 1.6 $g.cm^{-3}$ for highly compacted horizons. The variability of the bulk density is spatially organized: in the North-East part, the bulk density is lower, whatever the depth (from 0 to 40 cm). Figure 13 shows a high correlation between bulk density values and rock content. The spatial distribution of the bulk density is then links to the spatial distribution, of stone content.

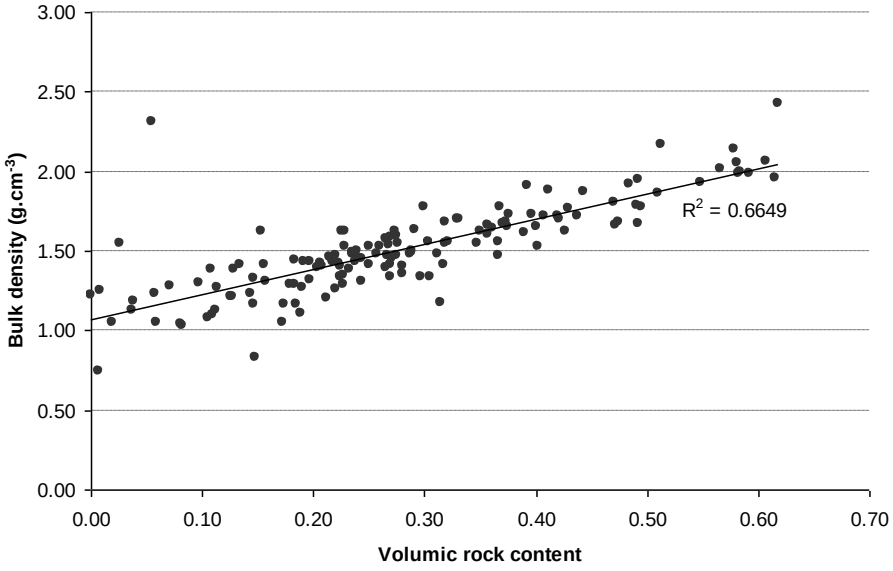

Figure 13 :Bulk density as a function of rock content

- Regional scale C content in the topsoil with airborne data

At the regional scale we considered a north-south transect of ~7 km width and ~60 km long (NW corner: 50°03'N 6°03'E; SE corner: 49°33'N 6°12'E), crossing 4 of the 5 agro-geological regions of the Grand-Duchy of Luxembourg (Figure 14). Airborne data were collected from this transect in which the field described above can be found (Stevens et al., 2010). Fifteen fields were retained (3-4 by agro-geological region) for intensive soil sampling (6 to 23 samples per field). Moreover, 83 additional samples were collected in 36 scattered fields (2-3 samples per field) to include, as much as possible, soil and spectral variability in the calibration models. A total of 325 soil samples were taken (49-97 samples in each agro-geological zone) for SOC analyses, 159 soil samples for moisture content as well as 3 measures of bulk density per field using 100 cm^3 cylinders. Bulk soil samples for SOC determination were composed of 10 sub-samples collected to a depth of 5 cm at random locations within a 7.5 m wide square centered on the geographical position of a sampling plot (recorded by a GPS receiver in differential mode). For moisture analyses, soil samples were taken randomly within the sampling plot in the very first millimeters (up to 1 cm) of the soil surface and put in hermetic plastic bag. Soil carbon of air-dried and sieved (2 mm) samples was analyzed by dry-combustion with a LECO CN analyzer. Soil moisture was determined gravimetrically. Ferrous oxide concentrations were measured on a subset of 21 field samples using dithionite extraction. For each of the 325 sample plots, the corresponding soil types were extracted from a 1/100 000 soil map of the Grand Duchy of Luxembourg containing 27 soil classes. Sampling plots belong to 11 soil classes, which can be reduced to 6 main textural classes (clay, loamy-clay, loam, sandy-loam, sand, colluvium and alluvium) and one marginal class containing only 2 samples (spring zone).

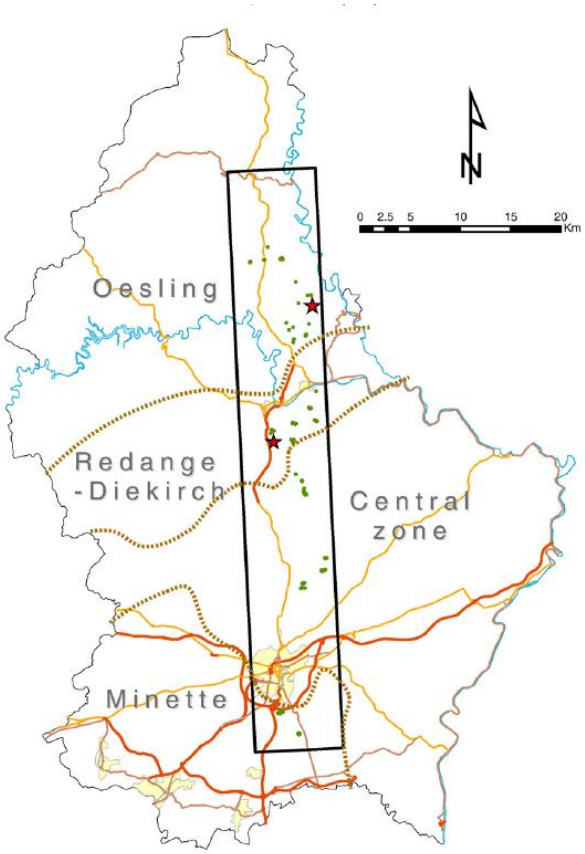

Figure 14 :Transect for which regional airborne data was collected. Dots indicate the fields that were sampled for calibration/validation

SOC contents vary from 7 to 61 g C kg^{-1} and differ markedly between soil types and agro-geological regions. For instance, soils of the Oesling area (North) contain, on average, more than twice the SOC content observed in the Minette area (South). Except for the Minette area, SOC contents show also a high variability within the same region, emphasizing the need for techniques able to measure SOC with a high spatial resolution. Large disparities can also be noticed when looking at SOC content as a function of soil type. Sand, sandy-loam and clay-loam soils exhibit a relatively low variation and contain less than 25 g C kg^{-1} while clay, colluvial-alluvial and loam soils may contain up to 40 g C kg^{-1} and present a large range of SOC contents.

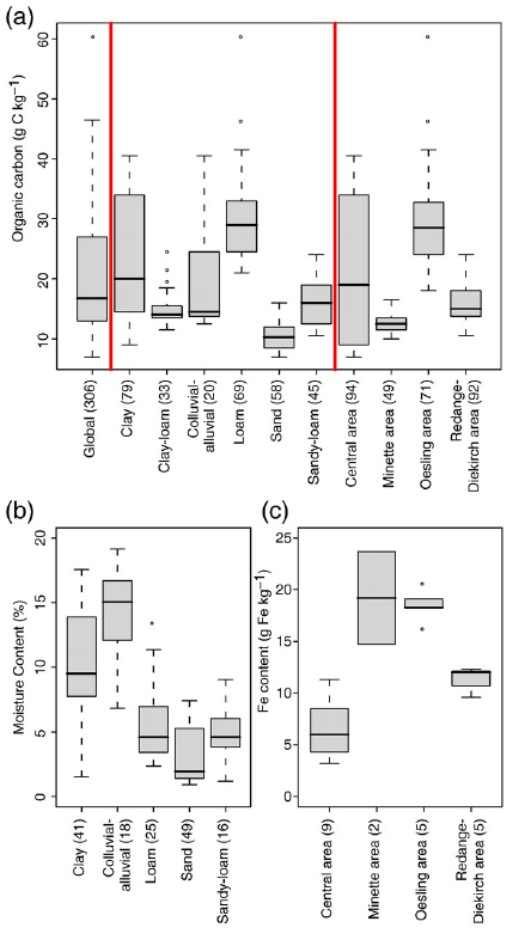

Figure 15 : Box and whisker plot of (a) OC content in g kg^{-1}. (b) gravimetric moisture content (%) and (c) ferrous oxides content in g Fe kg^{-1}. Number of samples in brackets.

Moisture content, as measured during the field campaign, was relatively low (median: 5.9 %, range: 0.9-19.1 %) and it varies greatly according to soil type (Figure 15a). Higher moisture contents were found in clay and colluvial-alluvial soils than in sand, sandy-loam and loam soils. While this relationship between texture and moisture content is likely to be valid, this can also partly result from the sampling protocol. A strong variation in ferrous oxides is also found between agro-geological regions, with soils of the Minette and Oesling areas having much higher contents than the ones in Middle and Redange-Dieckirch areas (Figure 15b). No correlation between Fe and OC content was observed (R= -0.17).

2.2. GEOPHYSICAL MEASUREMENTS REALIZED

2.2.1. Geoelectric

- Measurement report

Electrical resistivity measurements were obtained at the field scale by the use of the ARP device described in Figure 16 (Automatic Resistivity Profiling, Geocarta society). ARP system consists in simultaneous measurements of electrical resistivity for 3 investigation depths. This system is similar to the MUCEP device described in the D1.3 report. Only the distance between the current injection electrodes and the resistivity measurements electrodes of the V3 array is different: 1.7 m instead of 2.0 m.

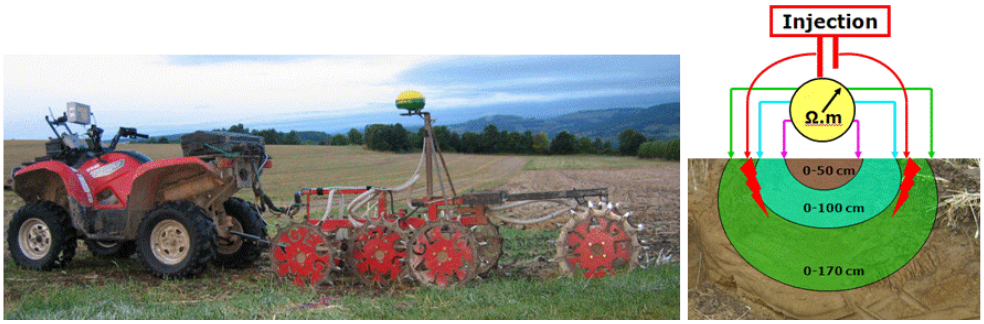

Figure 16 : Picture of the Automatic Resistivity Profiling and scheme of the measurement principle

The measurements were realized along transects separated by 1 m covering the entire field. Along one transect, measurements were performed and recorded every 10 cm. In addition, 5 vertical electrical soundings (VES) were realized at different locations in the plot (locations 2, 7, 12, 21 and 26 of the validation database). 10 electrode spacings were performed with the Wenner array: 0.1, 0.15, 0.2, 0.3, 0.4, 0.5, 0.7, 1.0, 1.5 and 2.0 m.

- Location map of measurements

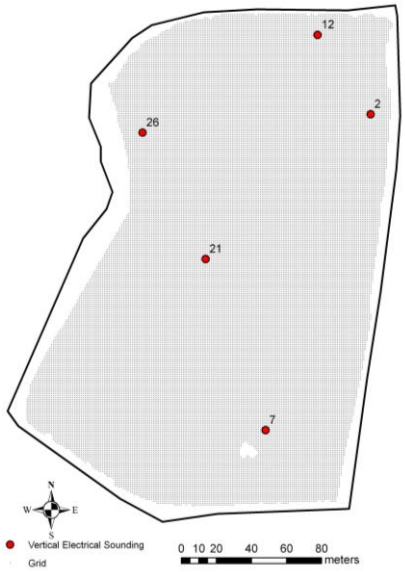

Figure 17 :Location map of the electrical resistivity measurements: grid of ARP measurements and locations of VES

  - Timetable and human effort: The electrical measurements were run on the field by two operators during one day for the ARP device and by two operators during one day for the VES.

  - Processing: The ARP raw data have been filtered by 9 median filters. The value of one data is replaced by the value of the median of the 9 values around if it is different of 40%. The data of the VES were

modeled from the sets of apparent electrical resistivity by a 1D inverse model (IPI2win software).

- Electrical resistivity map and VES results

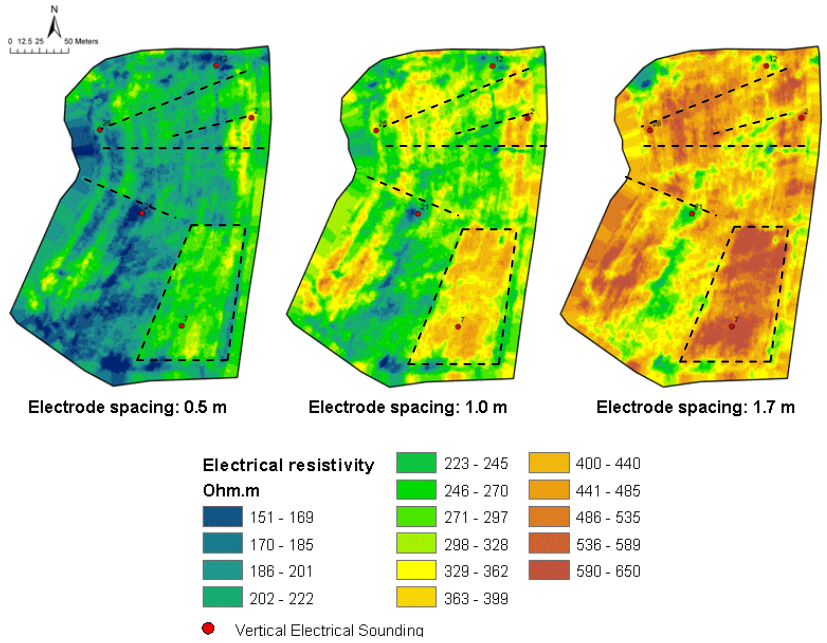

Figure 18 :Electrical resistivity map for the 3 investigation depths

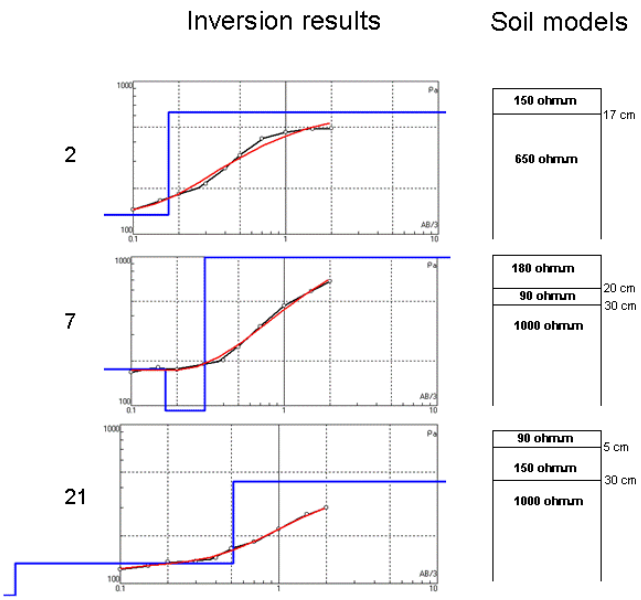

Figure 19 :Results of 1D inverse models from VES for locations 2, 7 and 21 and schemes of soil models obtained

The electrical resistivity map presents relatively high resistivity values: from 150 to 650 ohm.m and more. The higher the investigated volume, the higher the

resistivity. This can be explained by the high content of stone in the soil which increases from surface to deep layers (see pedological description previously).

The electrode spacing = 0.5 m shows resistivity values close to 150-200 ohm.m. The interpretation of VES puts into evidence the presence of a shallow layer (30 cm) of approximately 150 ohm.m. The electrode spacing = 1.7 m shows resistivity values close to 650 ohm.m. This is due to the influence of the deep layers which are very resistant as showed by the VES.

A rectangular pattern always more resistant is visible at the South-East part of the field, as well as straight lines in the thalweg region. Due to their position and orientations, these structures are definitely not due neither to the geophysical prospection, nor to the filtering process. They could be linked to actual or past anthropic activities. There is no visible slope effect.

- Stone content map

Electrical resistivity measurements with the ARP device are highly sensitive to the stone content. The latter leads to modifications of measurements due to two main reasons: on the one part, the direction of the current lines is highly modified and the soil behaves as a very heterogeneous porous medium, which leads to high uncertainties in the inversion of electrical resistivity data. On the other part, the contact of electrodes with the soil is very bad when the electrode is in contact with a stone, and the injection of current is not efficient. As a consequence, the resulting electrical resistivity signal contains a high level of noise, in all the three arrays of the ARP, and especially for the first array (electrodes spaced 50 cm apart). Tetegan et al. (2010, in progress) have demonstrated that the standard deviation of the electrical resistivity map are correlated with the stone content, when the latter is equal or higher than 20 % in volume in the surface horizon. A standard deviation map has been calculated by the following method: each pixel is of 50 x 50 cm in size, and its value is the standard deviation of the electrical resistivity values calculated in a circle centered on the pixel with a radius of 5 m.

Figure 20a shows the electrical resistivity standard deviation map of the first array. The values are comprised between 7 and 65 ohm.m. As expected, the standard deviation values were higher in the North-West part area where the stone content was high. Surprisingly, they were also higher in the North-East part (in the anthropogenic area), where the stone content was very low. Other effects do probably influence the signal but they will not be discussed here.

From the direct measurements of stone content, the mean value of the stone content in the 0-30 cm layer was calculated. Four locations were randomly chosen out of the anthropogenic part, and a relationship between the stone content in the 0-30 cm layer and the standard deviation of electrical resistivity values from the first array has been calculated Figure 20a). It was then used to translate the standard deviation map into a stone content map (Figure 20b). On the other locations, the stone content measured on soil cores was compared to

the stone content measured by the model. Except at some locations in the anthropogenic part, the estimation is rather satisfying.

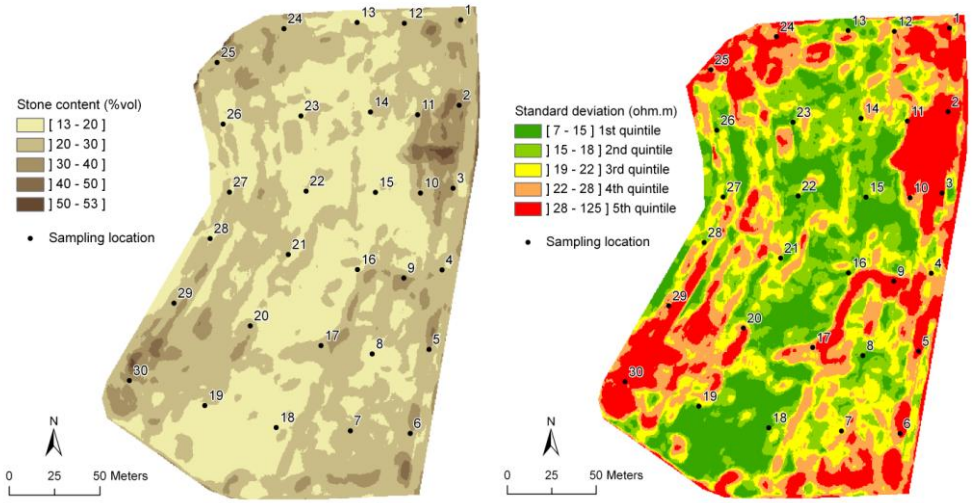

Figure 20 : Standard deviation of the electrical resistivity raw data (left) and modelisation of the stone content (right).

2.2.2. Seismic

- Measurement report

Seismic experiments on Luxembourg site led to realize 5 profiles covering around 5 ha for almost 200 seismic shots. In addition, 30 penetrometers were performed on the same area to validate the method.

  - Location map of measurements

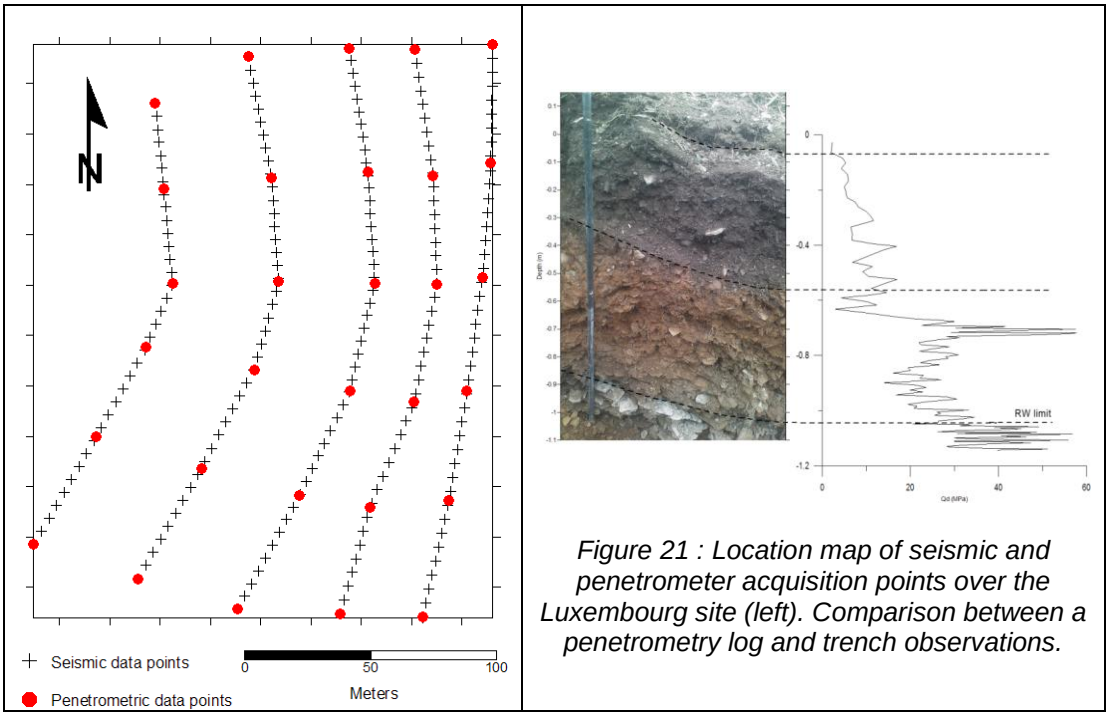

Figure 21 : Location map of seismic and penetrometer acquisition points over the Luxembourg site (left). Comparison between a penetrometry log and trench observations.

- Timetable and human effort: The Digisoil's seismic system was run on the field by two operators during two days; another day was dedicated to penetrometry measurements and trench observations.

- Processing: because of the low signal/noise ration observed on the surface wave dispersion diagrams, an alternative seismic processing was tested. This last one consisted in picking the P-wave first arrivals and inverting them in a 2D tomographic approach to obtain a Vp distribution in depth along the 4 profiles. Then, by analyzing a statistic multimodal velocity distribution, the velocity value corresponding to the limit between the soil and the mechanical bedrock is estimated and validated with the penetrometry data and trench observations.

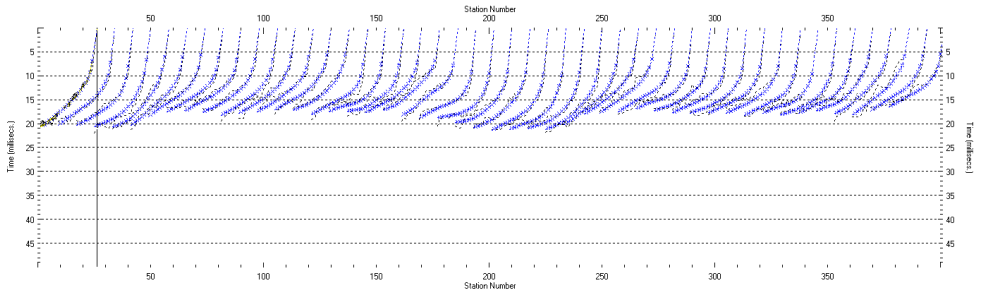

Figure 22 : representation of the P-wave fist arrivals data points used in the Vp inversion

- Presentation of the geophysical maps

The geophysical map was derived from the interpolation of 2D Vp tomograms obtained after P-wave first arrivals inversion.

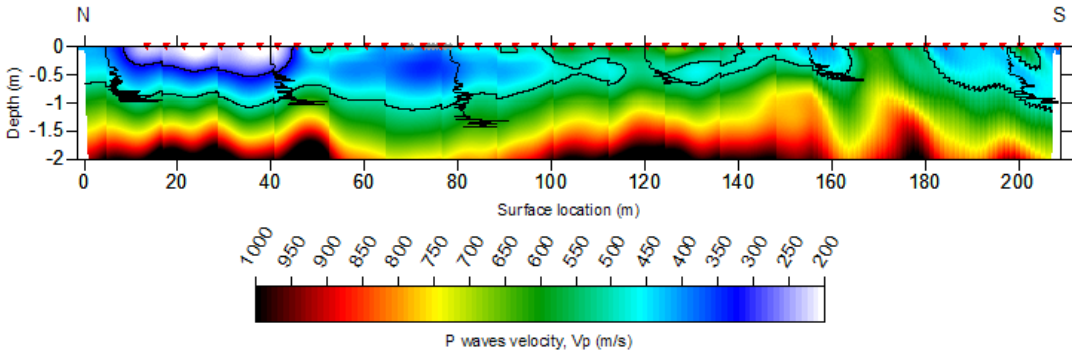

Figure 23 : exemple of 2D Vp section after P-wave first arrivals inversion. The black line represents the limit between the soil and the bedrock validated with the penetrometry data.

When interpolating all the dataset in a 3D velocity model, a map of the soil depth and soil velocity can be derived. These maps can be afterwards compared to the validation dataset, i.e., penetrometry, to estimate the a posteriori uncertainty related to the method.

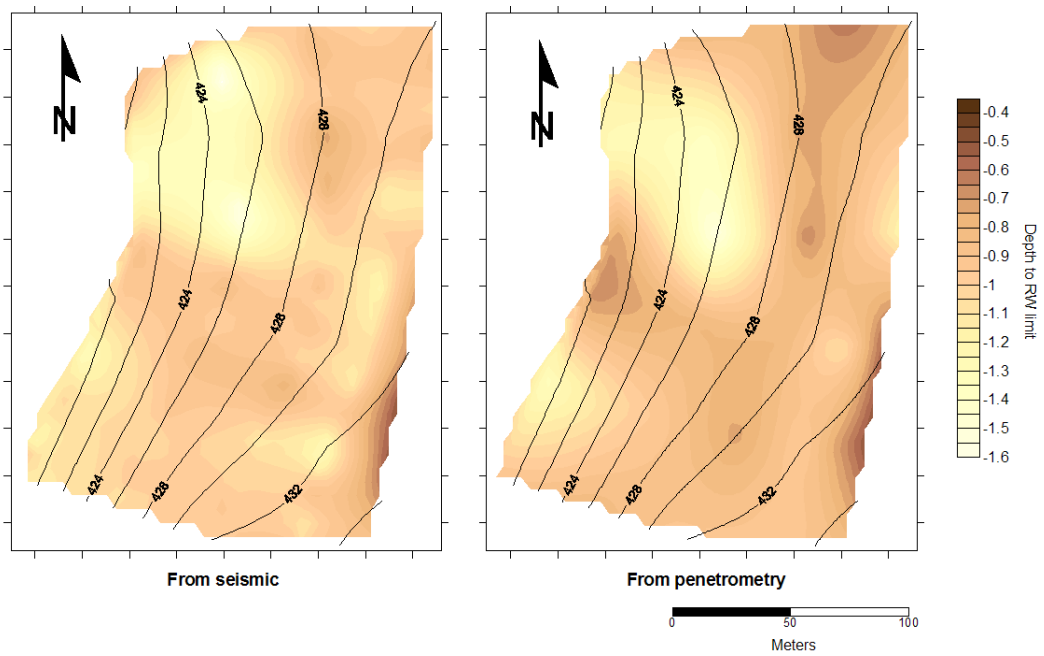

Figure 24 : Comparison between the soil depth obtained from seismic and penetrometry measurements.

- Spatial structure and data interpolation

The spatial structures of the soil depth was assessed from variograms estimated along four directions: 0°, 35°, 90° and 135° from geographic north. The variograms were generated from all possible sample pairs in a given direction grouped into classes (lags) of approximately equal distance (Matheron, 1965). The variance (one-half of the mean squared difference) of the paired sample measurements were then plotted as a function of the distance between the samples to provide a means of quantifying the spatial structure of the data. The soil depth obtained using seismic method was then interpolated by ordinary kriging - a geostatistical method that takes into account both the distance and the degree of variation between known data points and relies on the data's spatial correlation structure to determine the weighting values. Ordinary kriging has been shown to perform better for soil parameters than other available methods (e.g. Burgess et al., 1981; Myers, 1994). The interpolations were accomplished by fitting each of the various theoretical variogram models (Quadratic components with scale=0.0551, Length=185, anisotropy ratio=2 and anisotropy angle=23.08°) to the empirical isotropic variogram via the least-square method (Figure below). The best fit model was used for the interpolation. Data points were then interpolated to a regular 5×5m grid using a full second-order polynomial drift function, as is common practice. With the interpolation process, we then create an output grid of kriging standart deviations which brings informations about the interpolation error. The figure below shows that the minimum interpolation error (between 0.01 and 0.05m) is situated at the location of data points and the maximum interpolation error (between 0.05 and 0.1m) is located between data points.

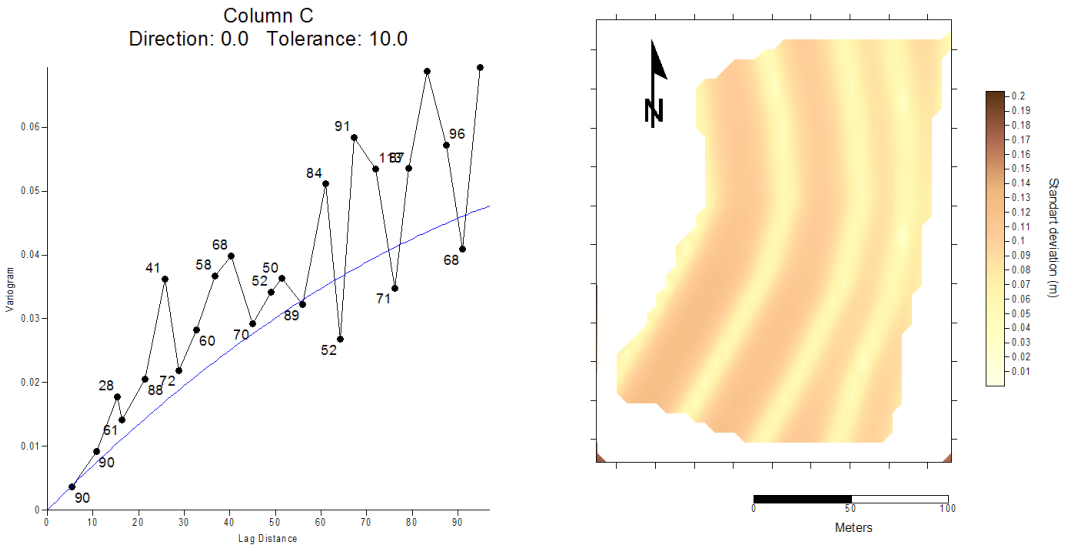

Figure 25 : (Left) Example of a vaiogram estimated in the direction 0° from geographic north. This variogram is fitted with a theoritical variogram model using a quadratic component with scale=0.0551, Length=185, anisotropy ratio=2 and anisotropy angle=23.08°, (Right) kriging standart deviation map.

2.2.3. Hyperspectral

- Work flow

The hyperspectral data acquired from the AHS 160 airborne sensor (section 2.2.3) produced the reflectance signal of the bare topsoil. This signal was then correlated with the C content of the plough layer (0-20 cm) as illustrated in Fig. 1.

- Calibration data and process

We sampled 27 topsoils (0-20 cm) in the selected and an adjacent field (Figure 26). The C content was determined as outlined in section 2.1.

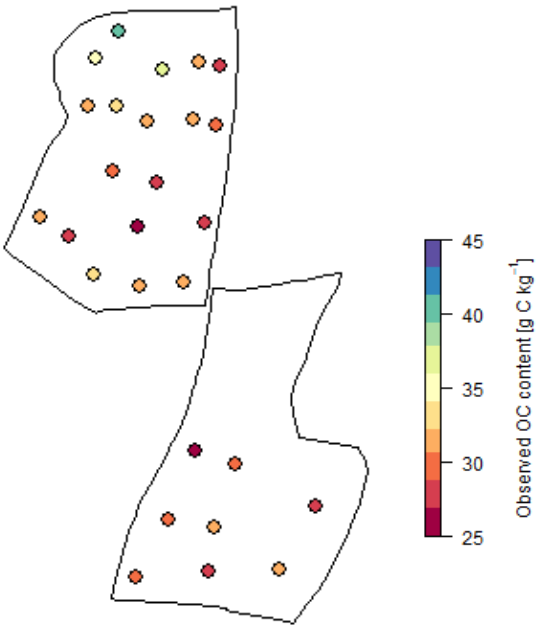

Figure 26 : Calibration points and their C content in the topsoil (0-20 cm)

Spectral data was analyzed with 2 different multivariate techniques: (i) Partial Least Square Regression (PLSR) and (ii) Penalized-spine Signal Regression (PSR). Statistical manipulations were carried out with the R software (R Development Core Team, 2007). We carried out the analyses for the visible and near infrared (VNIR : 400 -1100 nm) separately as well as for the VNIR combined with the shortwave infrared (SWIR : 1100-2500 nm).

A Principal Component Analysis was run prior to the PLSR to calculate for each spectrum the standardized Mahalanobis distance (H) to the average spectrum (Shenk and Westerhaus, 1991). Spectra with a H > 3 (X-outliers) were removed. In order to avoid the problem of overfitting, a critical step in the algorithm is the determination of the appropriate number of Latent Variables. This is usually determined by minimizing the value of the Predictive Residual Sum of Square (PRESS) by leave-one-out cross-validation. While in PLSR the order of predictors (i.e. wavelengths in spectroscopy) has no influence on the model, PSR forces the

coefficient of the regression to vary smoothly across the wavelengths. This is done by projecting the coefficients onto a set of smooth functions (B-splines). The smoothness is controlled by imposing a penalty on the difference between adjacent B-spline coefficients. Several PSR parameters must be fixed, of which (i) *d*, the order of penalty difference (usually between 0 and 3), (ii) the degree of B-splines and (iii) the number of intervals between knots (the point where B-splines join). After several tests, it was found that better results were obtained with *d* = 3, degree = 4, and intervals = 5.

- C content maps at the field scale

The spectral models produced the best results for the PSR technique applied to the spectra covering the VIR and SWIR (400-2500 nm; Figure 27). The spectra were calibrated and validated against the C content in the upper 20 cm of the soil. This corresponds to a homogenous C content in the ploughlayer. We excluded one outlier in the validation, as the spectra of the sample point close to the field border was influenced by the neighboring grassland. The PSR on the VNIR-SWIR proved to be the best combination of technique and spectral range.

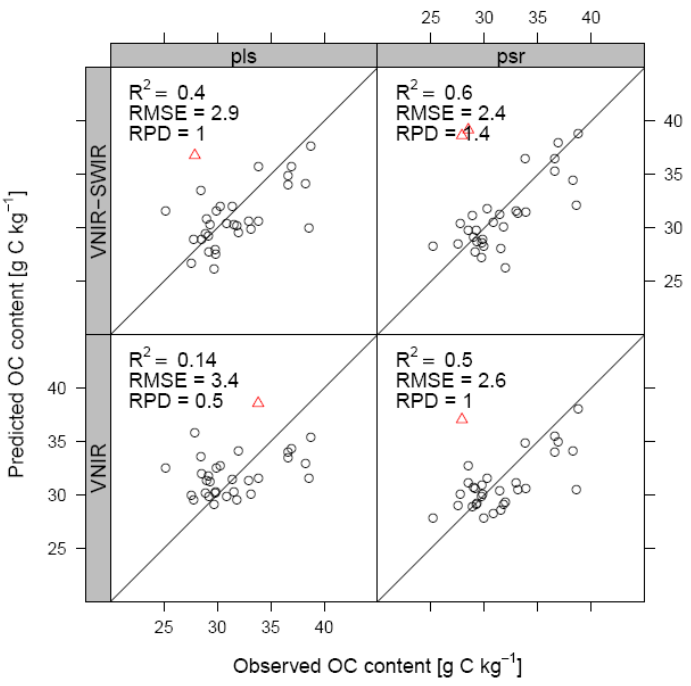

Figure 27 : Validation of the hyperspectral technique against C content in the upper 20 cm. Two techniques (PLSR and PSR) and two spectral ranges (VNIR 400-100 nm and VNIR-SWIR 400-2500 nm) were used.

The C content in the ploughlayer decreased from the northern border and the thalweg to the southern part of the field.

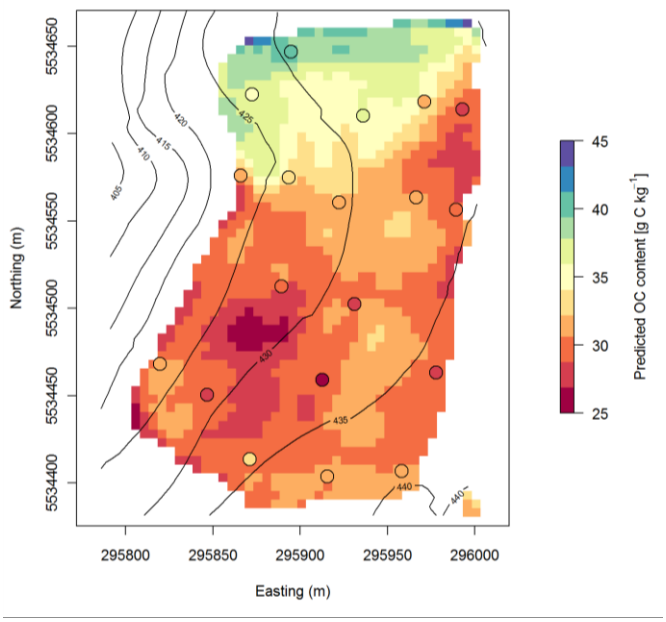

Figure 28 : Map of the C content in the plough layer (0-20 cm).

- C content maps at the regional scale

Stevens et al. (2010) carried out an independent validation of the regional scale spectral models (see section 2.1 regional airborne data). The models are somewhat less accurate than the field scale model with an RMSE ranging from 4.5 to 5.4 g C kg^{-1} and an RPD from 1.31 to 1.75 (Figure 28).

In general separate models for each soil type or agricultural region perform best for the full spectral range.

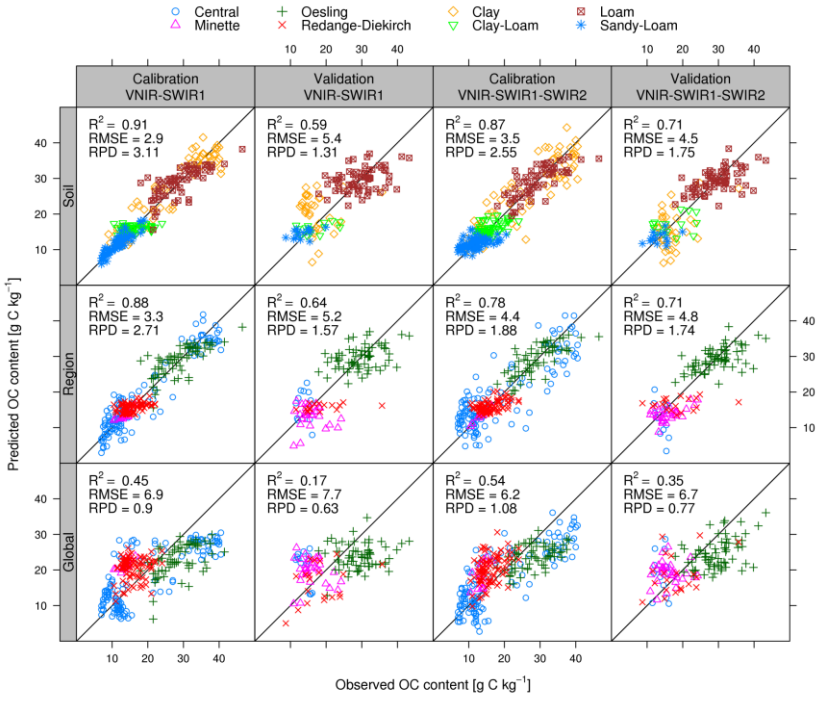

Figure 29 :Calibration and validation of spectral models applied to predict C content in bare top soils at the regional scale.

2.2.4. EMI

Electromagnetic induction (EMI) data were acquired with two sensors: the EMP-400 Profiler (GSSI) and the EM38 (Geonics). The Profiler was carried by the user and allowed to perform measurements at three frequencies (5, 10 and 15 kHz), simultaneously. In contrast, the EM38 was mounted on a quad used as a platform for both GPR and EMI measurements (Figure 30).

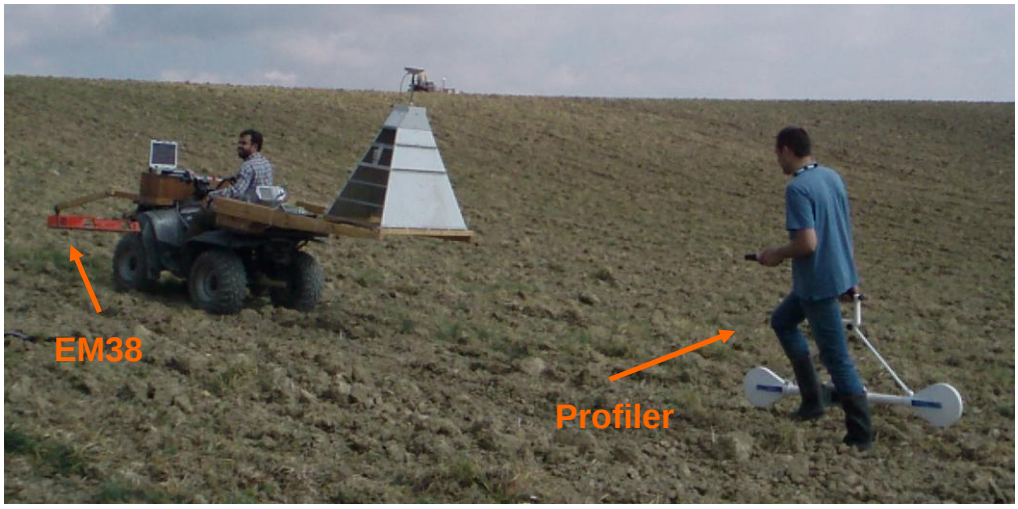

Figure 30 : EM38 and EMP-400 Profiler setup for EMI measurements.

- Measurement report
    - Location map of measurements

EMI measurements were carried out along transects spaced approximately 15 m apart, with one transect on two passing close to the locations of the ground truth measurements. The resolution (measurement spacing) within the transects was about 1 m. Several sets of measurements were performed over two days: the 6th and the 7th of September 2010. These two dates are characterized by contrasted soil moisture states with relatively dry soil conditions on the first day and higher soil water content on the second day, as a result of a rain event that occurred during the intermediate night. The studied field was mapped three times with each sensor. For the Profiler, data were collected with horizontal dipole orientation on the first day, and with both vertical and horizontal modes on the second day. For the EM38, all measurements were performed with vertical dipole orientation, one time on the 6th of September and two times on the 7th of September (Figure 31).

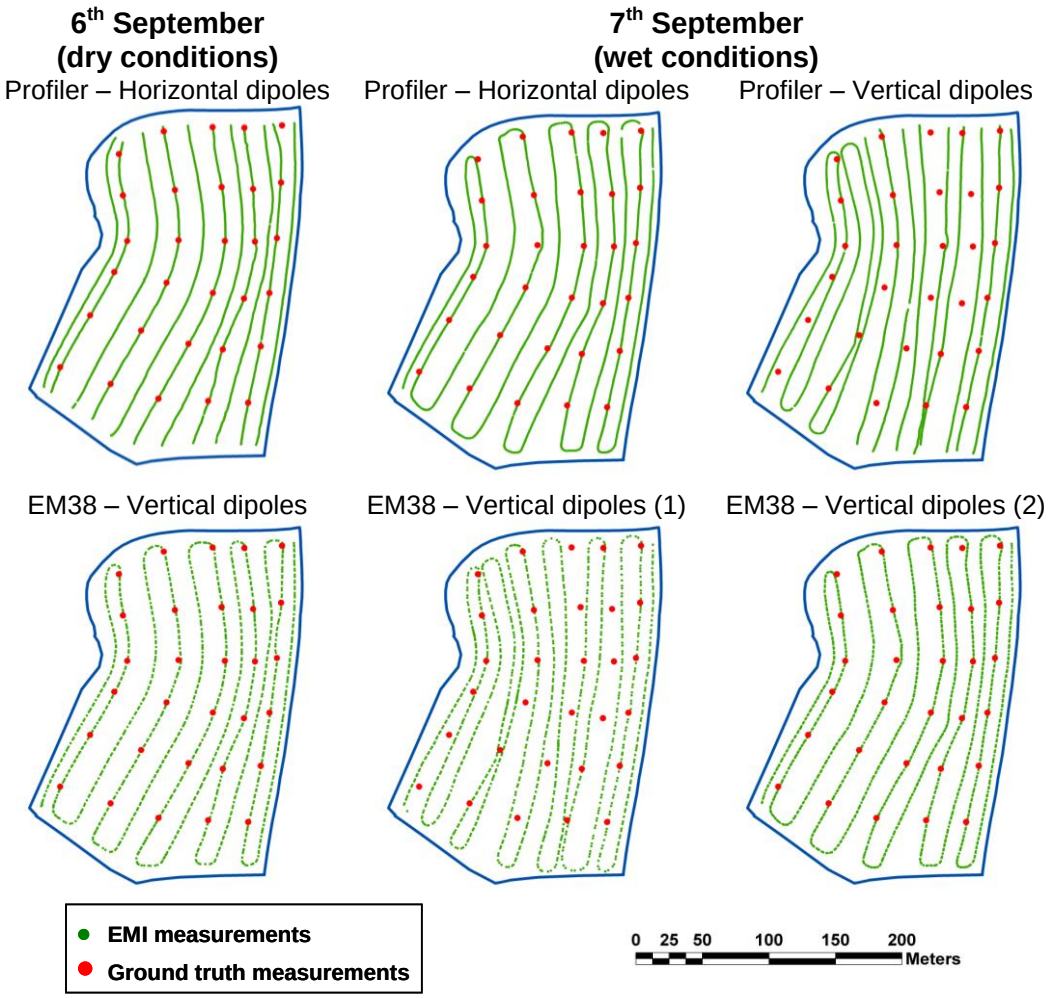

Figure 31 : Location of the EMI measurements over the Luxembourg site for the two measurement dates, for each sensor and for each orientation mode.

- Timetable and human effort: With the EM38, on average 0.75 hour was necessary for one person to collect each data set. For the Profiler, carried at walking speed over the area, the time needed to perform each measurement set was about 1.25 hour. The total area of the study field is around 5 ha.

- Processing: The two EMI sensors used in this field campaign provided directly soil apparent electrical conductivity values, which where standardized according to the reference temperature of 25°C using the equation proposed by Sheets and Hendrickx (1995) :

$$\sigma_{25} = \sigma\left(0.447 + 1.4034 e^{-T/26.815}\right)$$

where σ_{25} (Sm^{-1}) is the standardized soil electrical conductivity at a temperature of 25°C and T (°C) is the soil temperature. For this site, the average measured soil temperature was 14.3°C (at a depth of 30 cm).

- Geophysical maps

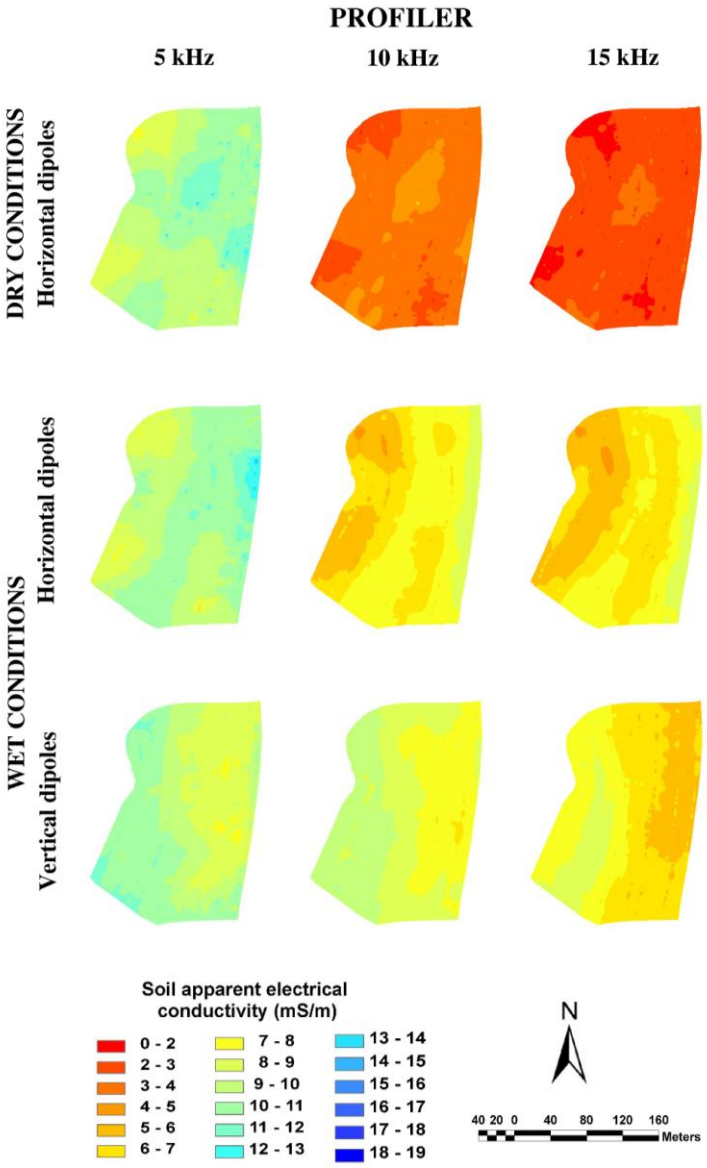

Figure 32 : Maps of the soil apparent electrical conductivity measurements performed with the EMP-400 Profiler sensor over the Luxembourg site.

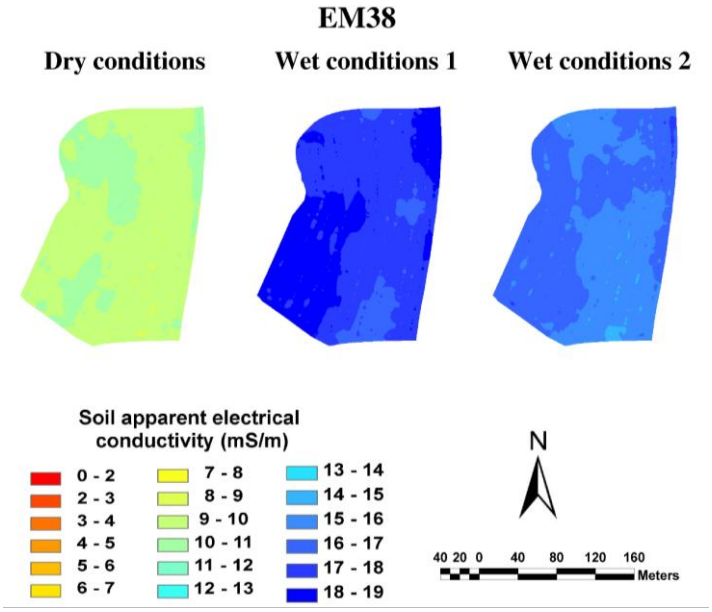

Figure 33 : Maps of the soil apparent electrical conductivity measurements performed with the EM38 sensor over the Luxembourg site.

Figure 32 and Figure 33 present the interpolated maps (inverse distance weighting) of soil apparent electrical conductivity measurements performed with the Profiler and the EM38 systems, respectively. The soil electrical conductivity is relatively low (< 20 mS/m) all over the area and, for a given data set, the range of variation is quite limited while pronounced differences are observed when comparing data from both sensors, from both dates and, for Profiler, from both orientation modes.

Regarding Profiler data, for both soil moisture conditions and each orientation mode, measured soil electrical conductivity tends to decreases as the frequency increases, particularly from 5 kHz to 10 kHz. This denotes a general increase of electrical conductivity with depth, from about 1 to 2 meters. In contrast, ERT data (see above) show a decrease of conductivity with depth. The origin of this discrepancy may be threefold: (1) different characterization depths of the instruments, (2) EMI calibration limitations, and (3) soil stratigraphy (shallow bedrock). Future analyses of the ground-coupled GPR data should permit to elucidate these questions. Rather good agreement is observed between the spatial patterns of soil electrical conductivity measured in horizontal dipole mode and the distribution of the soil types within the area, more particularly when we examine the data from the second day (wet conditions). In particular, the eastern limit of the field tends to show relatively higher values for soil electrical conductivity, corresponding to the presence of the Anthrosol, while, at the western limit, higher soil electrical conductivity values tend to be observed around the location of the Cambisol. Moreover, a more general west-east gradient of soil electrical conductivity is also observed in accordance with the topography. For horizontal dipole mode, soil electrical conductivity generally tends to increase

from the western limit to the eastern limit of the field, namely, as elevation increases, while the opposite trend is found for vertical dipole measurements. The generally higher soil depth in the western part of the field compared with the eastern part would partly explain these observations, the vertical dipole mode being more sensitive to the deeper soil layers than the horizontal dipole mode and the electrical conductivity of rocks tending to be lower than that of soil. Furthermore, these patterns of soil electrical conductivity would also be partly ascribed to the higher clay content of the shallowest soil layer (0-10 cm) in the western part of the field by comparison with the eastern part, and inversely for the 20-30 cm layer. Finally, comparing horizontal dipole measurements of both days, we observe an increase of soil electrical conductivity from the first day to the second day, namely, as the soil water content increases. This is particularly pronounced for the 10 kHz and 15 kHz frequencies, which correspond to the shallowest investigation depths.

For EM38, soil electrical conductivity also increases from dry soil conditions to wet soil conditions, while only very small differences are observed when comparing both data sets from the second day of measurements.

It is worth noting that these commercial sensors provide only semi-quantitative values of soil electrical conductivity, as a result of a lack of robustness of their calibration which affects measurement repeatability (see Lambot et al. (2009)). Therefore, a part of the differences in absolute values of soil electrical conductivity observed between data obtained from different calibrations may be ascribed to these calibration issues. This refers to the data from Profiler, for which a new calibration had to be performed at the beginning of set of measurements, as well as to the comparison of Profiler and EM38 data. In contrast, the three data sets from EM38 are directly comparable as the calibration of this sensor was not modified during the field campaign. These issues will be fixed by correcting the soil electrical conductivity values using a more robust calibration procedure, based on ERT data (Moghadas et al., 2010).

2.2.5. GPR

2.2.5.1 Off-ground GPR

The combination of a Vector Network Analyzer (VNA) and a horn antenna (200-2000 MHz) located at 1.1 m height, was used to perform the off-ground measurements. The system was mounted on a quad and a differential GPS was used for data geo-referencing. The data acquisition was controlled by a portable computer which recorded measurements every 1 second (Figure 34).

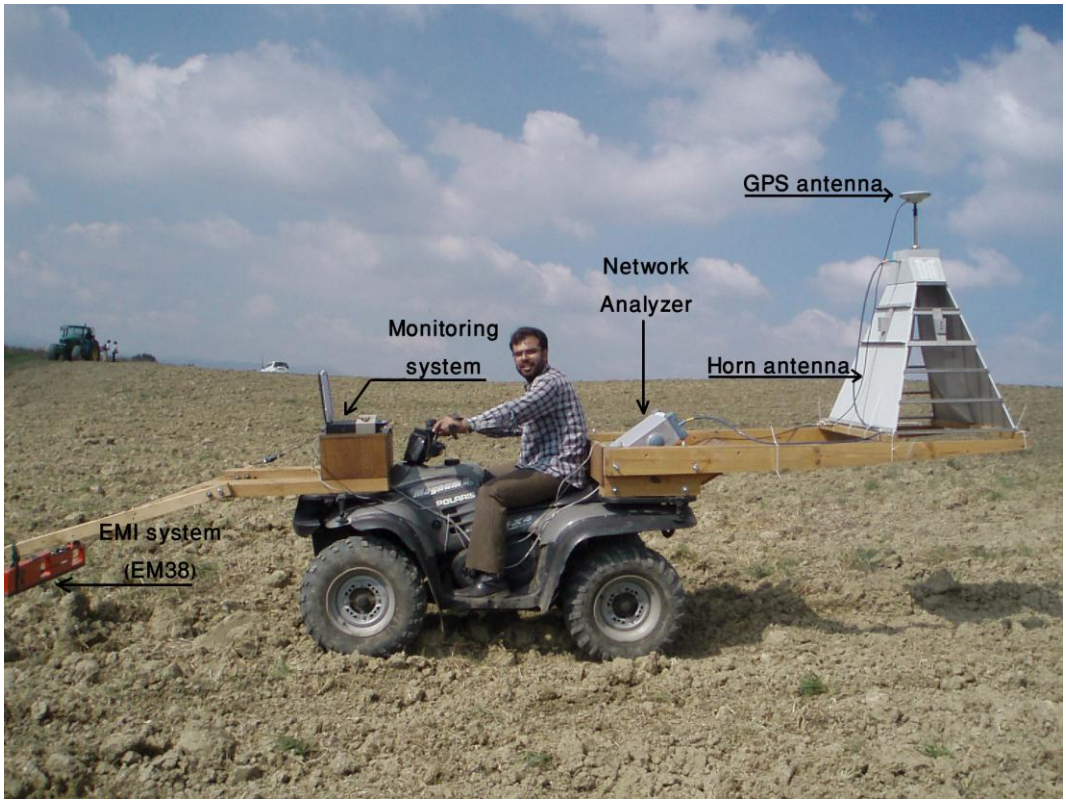

Figure 34 : Picture of the off-ground GPR system.

- Measurement report
    - Location map of measurements

The measurements were repeated during two days over the entire study area because of variation of the weather conditions. The weather was dry during the 1st day, while rain occurred on the 2nd day, resulting in an increase of the shallow/surface soil moisture. The measurements were performed along S-N and N-S transects at the same locations as the EM38 measurements (Figure 30).

- Timetable and human effort: For proper high-resolution mapping of soil properties, off-ground GPR measurements should be carried out at a velocity lower than 2 m/s. On the Luxembourg site, the average velocity of the platform during the measurements was 1.9 m/s Therefore, each coverage of the total field area took between half an hour and one hour for one person.

- Processing: GPR data were inverted using the model of Lambot et al. (2004, 2006), as fully documented in Grandjean et al. (2009) (section 3.2.1). The retrieved dielectric permittivity is shown in Figure 35 for both the dry and wet days using kriging interpolation.

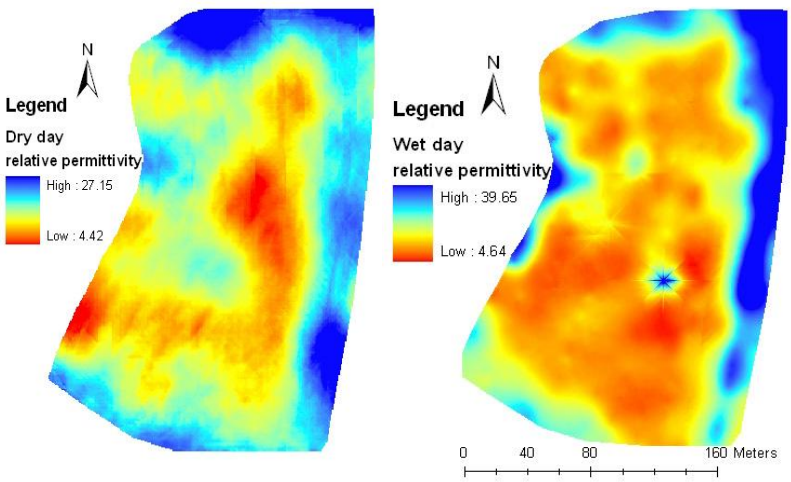

Figure 35 : Relative dielectric permittivity of the shallow soil retrieved from off-ground GPR data inversion.

2.2.5.2 On-ground GPR

We used a time-domain GPR system (model SIR-20, Geophysical Survey System, Inc., GSSI, Salem, Massachusetts, USA) combined with a pair of 400 MHz shielded bow-tie antennas located at 1.1 m distance from each other as an impulse radar (Figure 36). Applying the two antennas allowed to use the monostatic and bistatic modes simultaneously.

Figure 36 :On-ground GPR system (SIR-20 using a pair of 400 MHz shielded bow-tie antennas with 1.1 m offset).

- Measurement report
    - Location map of measurements

On-ground GPR measurements were performed following the same transects as for the off-ground radar measurements.

- Timetable and human effort: For GSSI system mounted on the quad only one person is necessary to drive and control the system. The survey velocity can be more than that for off-ground GPR (maximum 2 times more). The complete field measurements took around half an hour.

- Processing: A power gain function of time with a factor of 2.5 was applied to better observe the later reflections compared to the surface reflection after cancelling the system gain and the background noise was removed for focusing on the bedrock reflection. As an illustration, Figure 37 shows one of the on-ground profiles which has been taken in the dry day survey, on which the bedrock reflection is clearly visible.

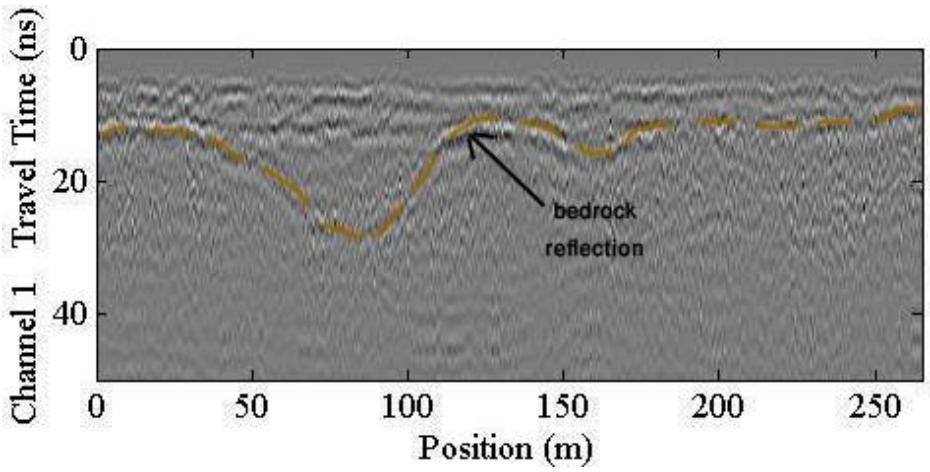

Figure 37 : On-ground GPR scan (N-S orientation 24 m away from the road)

2.2.6. Magnetism

- Measurement report

The magnetic properties measurements were located on 231 datapoints (see location on Figure 38). The magnetic susceptibility was measured with 2 devices in 4 configurations (Bartington MS2D, CS60 VCP, CS60 HCP and CS60 VVCP). The magnetic viscosity was measured with 3 devices (ELSIEC DECCO, Protovale TS6 and VC100).

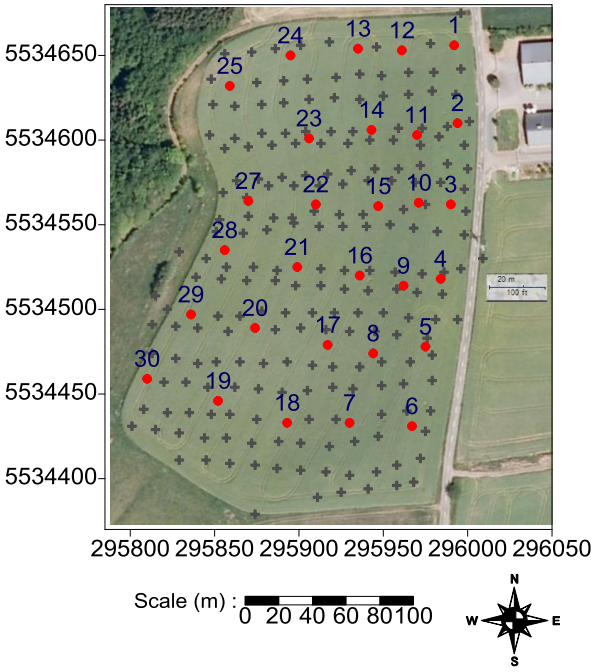

Figure 38 : Location of the measurements points on the studied zed field (grey cross). The red dots indicate the sampling points were the validation cores have been taken

- Timetable and human effort

The devices were handled separately by a 2 person team. It takes about half a day to measure all the data points with each device.

- Processing (summary)

The data have been filtered by 5 by 5 median filter. A calibration relationship has been applied to obtain the apparent magnetic properties maps.

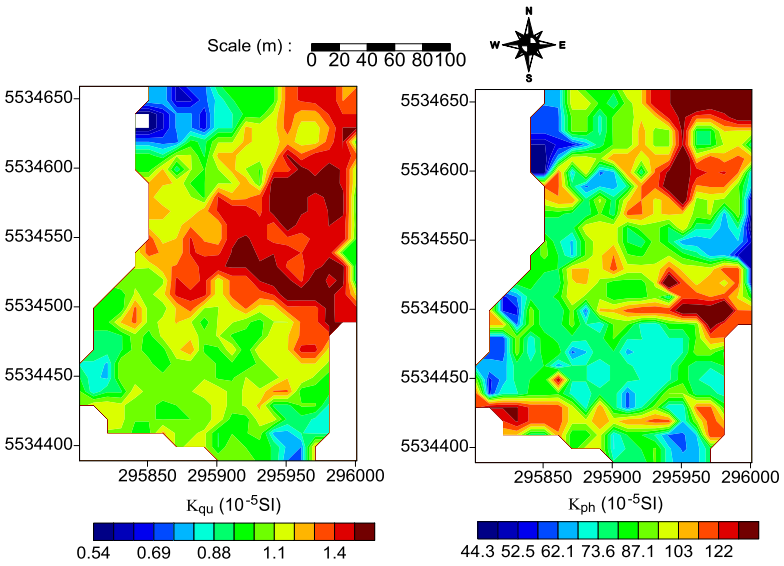

a) b)

Figure 39 : DECCO apparent magnetic viscosity map (a) and MS2 apparent magnetic susceptibility map (b) obtained on the site

- Magnetic maps

Apparent magnetic viscosity measured with the DECCO (Figure 39) shows three zones:

- The first one on the NW part of the field exhibiting low values
- The second one, on the East and NE part of the field showing stronger values
- The third one, on the South part of the field presenting intermediate values

Apparent magnetic susceptibility measured with the MS2D (Figure 39) shows two major trends:

- The first one exhibits the values falling down from East to West and seem to be linked to the topography
- The second one consists in the values lowering down from North to South

The two maps are in good agreement. Nevertheless, the differences should suggest some zones present ferrimagnetic small single domain grains in higher concentrations, because magnetic viscosity is only sensitive to this parameter.

- Water content maps

Focusing on the ground surface reflection in the time domain, ínversion of the GPR model developed by Lambot et al. (2004,2006) allowed to retrieve the dielectric permittivity of the shallow soil. Based on these estimates of the dielectric permittivity, the Topp (1980) equation was then used to determine the corresponding water content. Figure 40 presents the kriged water content estimates for the dry and the wet days of measurements. This figure shows good correlation between the estimated water content and the field conditions (dry vs. wet). Figure 41 shows the estimated water content using GPR and kriging versus volumetric sampling. Results are consistent but significant differences can be observed. These are to be attributed mainly to the different locations of the volumetric samples with respect to the radar measurements (kriging errors) and the different characterization scales given the significant variability with space of soil moisture (heterogeneity at a scale < 1 m).

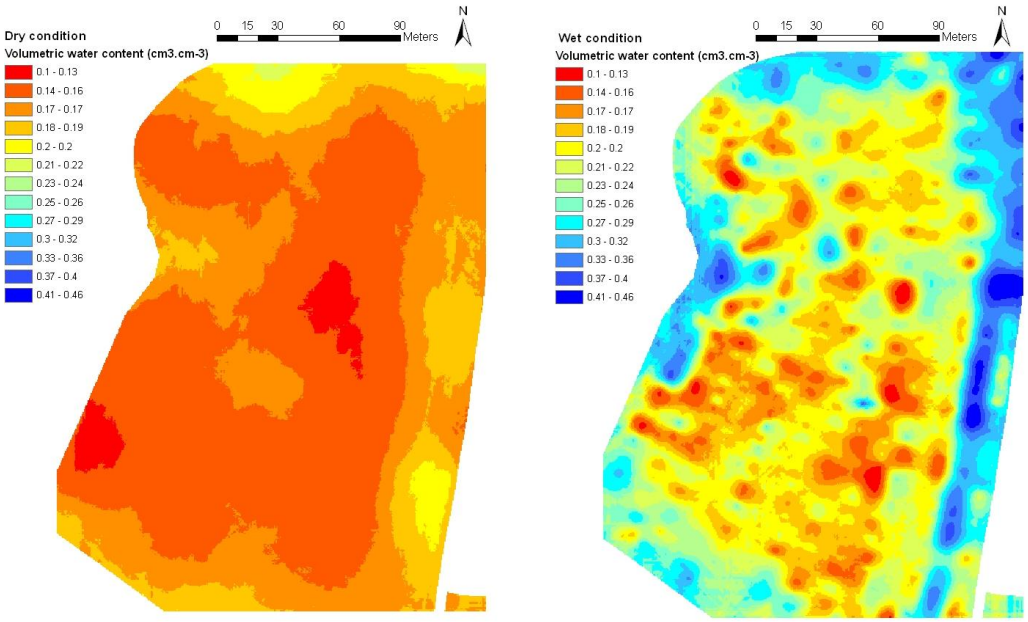

Figure 40 : Water content estimates from off-ground GPR measurements at the Luxembourg site

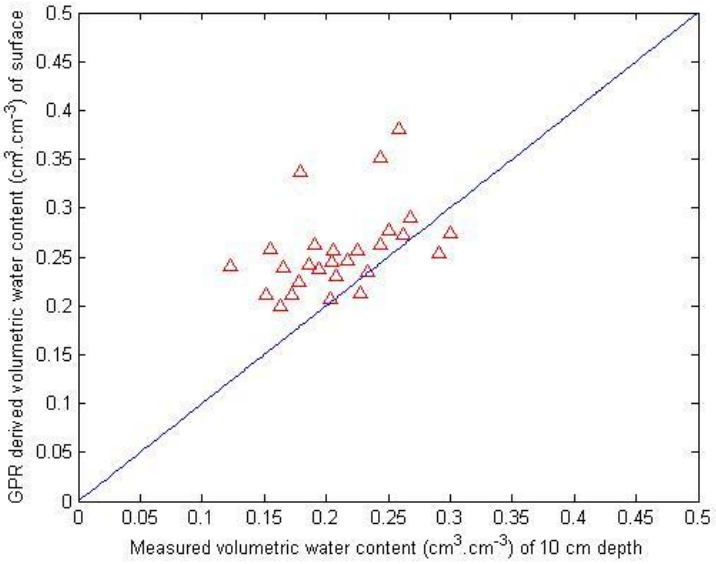

Figure 41 : Water content estimated from off-ground GPR measurements and kriging versus volumetric sampling at the Luxembourg site (wet conditions only)

- Clay content map

Soil electrical conductivity of low-salinity soils is mainly affected by soil water content and clay content. Rhoades et al. (1976) proposed the following empirical model to relate soil electrical conductivity to soil physico-chemical properties:

$$\sigma = a\theta^2 + b\theta\sigma_w + \sigma_s$$

where σ is the bulk soil electrical conductivity (S.m^{-1}), θ is the soil water content (m³.m^{-3}), σ_w is the soil solution electrical conductivity (S.m^{-1}), σ_s is the electrical conductivity of dry soil (S.m^{-1}), and *a* and *b* are soil specific empirical parameters. In this equation, σ_s may be expressed as a function of the soil clay content. We used this model to estimate clay content from EMI measurements considering empirical parameter values (*a*=1.382, *b*=-0.093) found by Rhoades et al. (1976) for a soil comparable to that of the main soil unit observed at the study site and assuming σ_w = 0.05 S.m^{-1}. Water content estimates from GPR measurements were used to remove the effect of θ on measured soil electrical conductivity and provide estimations of σ_s. For a subsample of the ground truth points, relationships were then established between σ_s estimates and clay content measurements. Finally, these calibration relationships were applied to estimate soil clay content at each EMI measurement point and we compared these estimations with the complete ground truth measurement data set.

For clay content within the 0-10 cm soil layer, these analyses were performed using horizontal dipole measurements as they present high sensitivity to the soil surface properties. Data sets from the two measurement days were considered in order to compare clay content estimates using data from contrasted soil water content conditions. For clay content below the plough layer (20-30 cm), vertical dipole measurements were used as this configuration presents higher sensitivity to the deeper soil layers, only one set of EMI data (second day of measurements) is available in this case. Figure 42 presents the calibration relationships established between σ_s estimates and clay content, and the comparison between the clay content estimations from these relationships and the ground truth measurements. The corresponding maps of clay content estimates over the site are shown in Figure 43. For the 0-10 cm layer, both a stronger calibration relationship between clay content and σ_s estimates and a generally closer agreement between clay content estimates and ground truth measurements are found for the wet soil conditions compared with the dry conditions. Such results would be explained by more contrasted patterns of soil electrical conductivity over the area under wet than under dry conditions, which would allow to better retrieve spatial variations of clay content. Nevertheless, in both cases, very poor agreement is observed between measurements and estimates of clay content at the location of the anthropogenic soil (represented by the orange dots in the graphs). The very different nature of this soil compared with the rest of the studied field may explain these observations, the values of the model's empirical parameters being soil-specific. Regarding the 20-30 cm layer, rather poor agreement is found between clay content estimations and measurements,

especially within the north-east part of the field where large overestimations of clay content are observed. Such discrepancies sometimes found between ground truth and estimates may at least partly arise from the fact that EMI measurements integrate a large volume of soil while clay content was determined from relatively small samples characterising a rather thin (10 cm thick) layer of soil. Furthermore, the rather low clay content at the study site associated with its narrow range of spatial variation over the investigated area also limit the accuracy of the estimations of this soil property from soil electrical conductivity measurements.

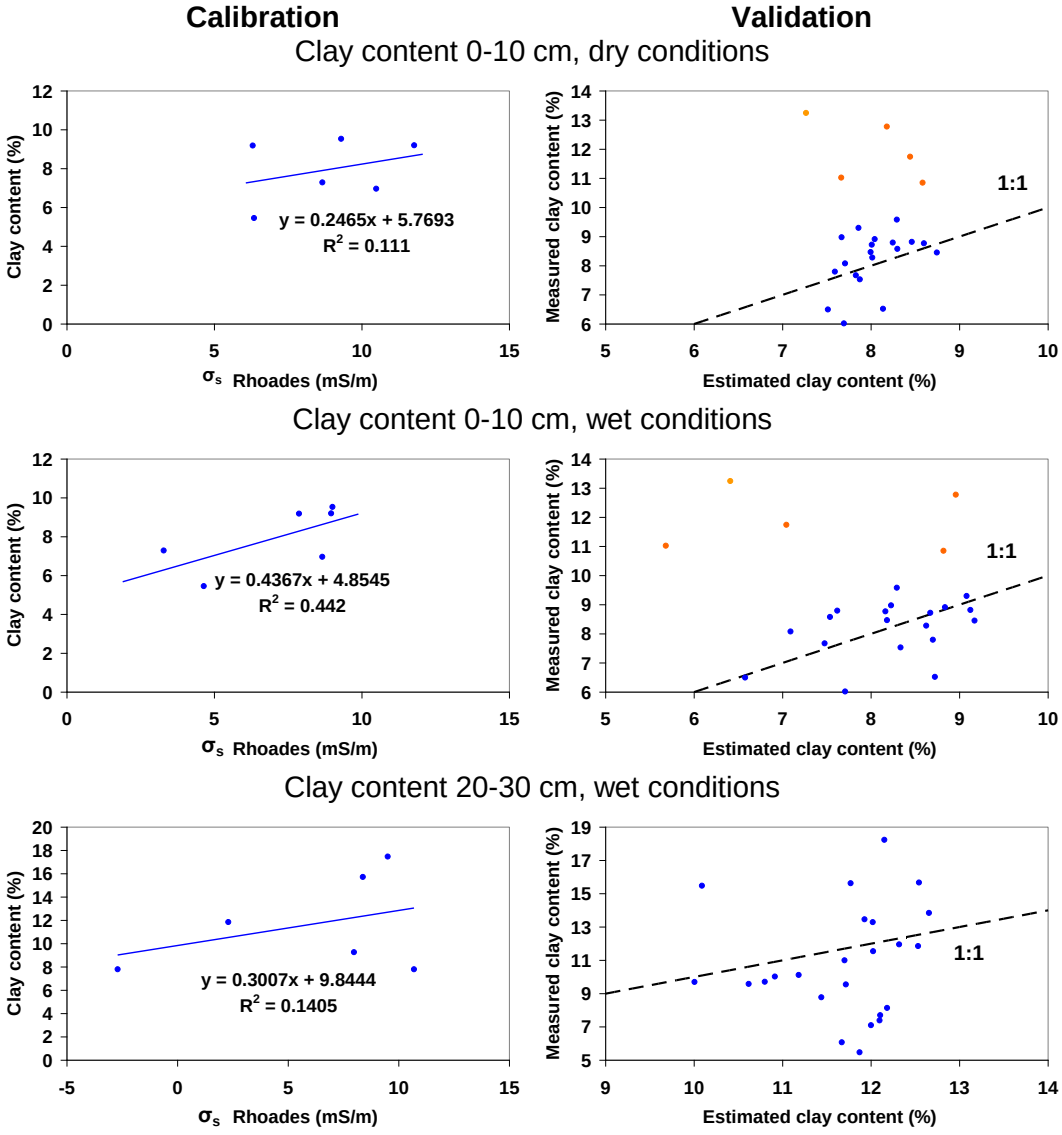

Figure 42 : Estimation of the clay content from soil electrical conductivity measurements. Calibration of the model on the basis of a subsample of ground truth measurements and validation of the model. The orange dots, far from the 1:1 line, correspond to points located in the anthropogenic North-West part and the clay content at these locations could not be estimated by the model.

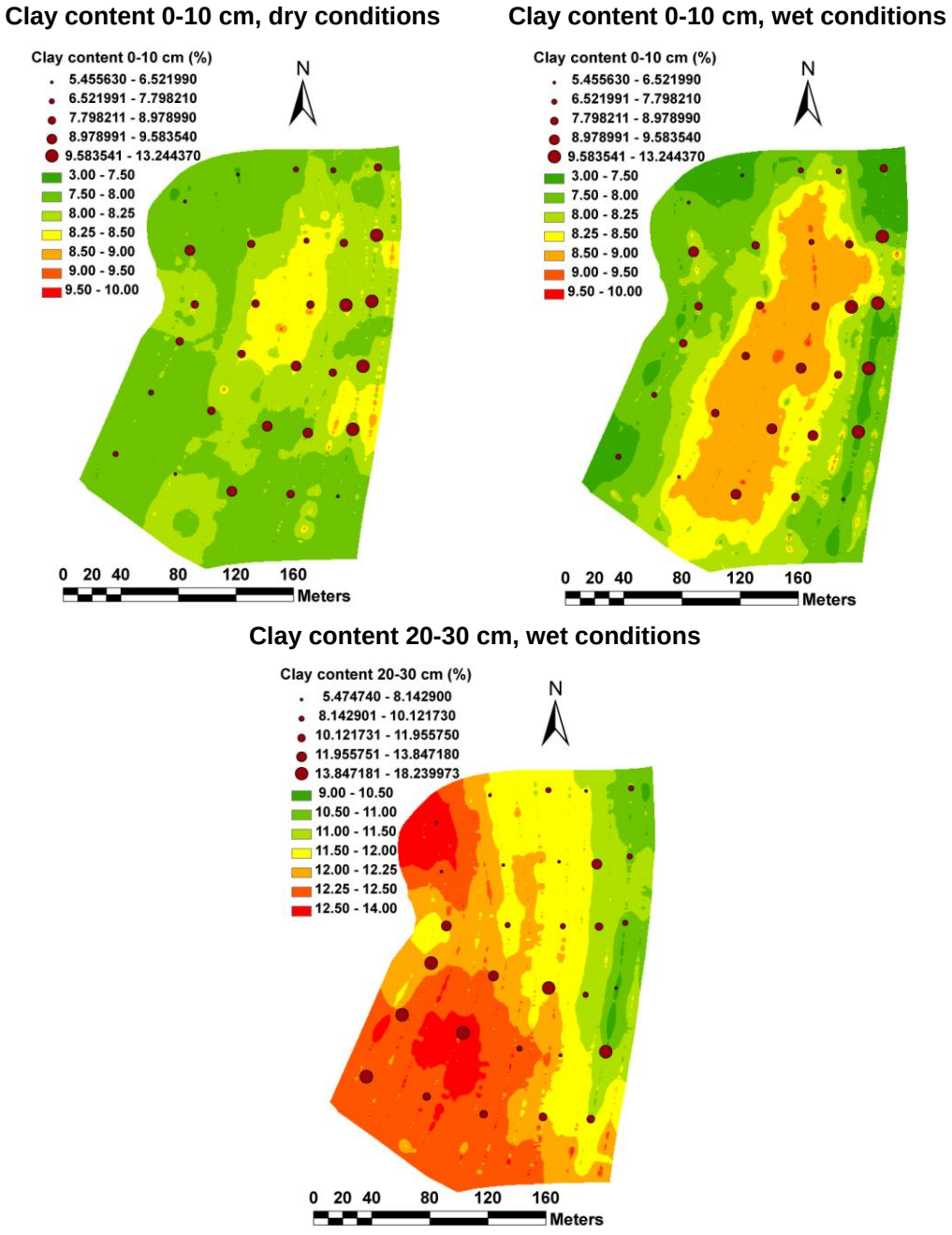

Figure 43 : Estimations and ground truth measurements of clay content over the Luxembourg site

3. Mugello site

3.1. SITE LOCALISATION AND PRESENTATION OF THE STUDIED AREA

The test area is located in the Mugello basin (Figure 44) (WGS84 coordinates approximately: Lat. = 43°58.6 N, Long. = 11°21.9 E), about 30 km north of Firenze and it is extended for about 20 km^2 to the north of the Sieve stream, left tributary of the Arno river, being comprised between the villages of Borgo San Lorenzo, Luco di Mugello and Scarperia. The landscape is typical of Tuscany intermontane basins, with gentle hills with low-altitude moderately dipping or level surfaces of alluvial origin as well as fairly- to highly-inclined downs (Figure 45).

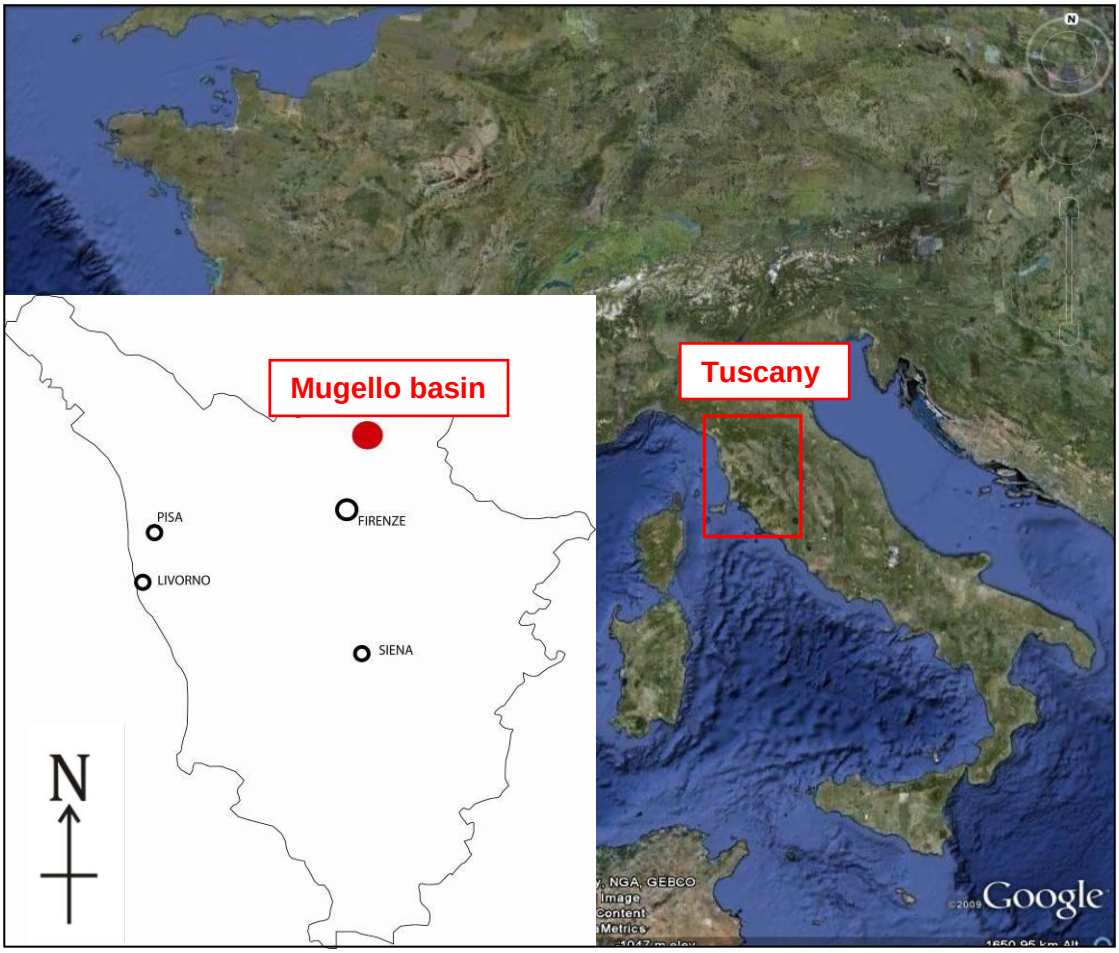

Figure 44 : Location of study area (Mugello basin).

Figure 45 : Landscape and view of the parcels sampled in Mugello basin.

3.1.1. Pedologic context presentation

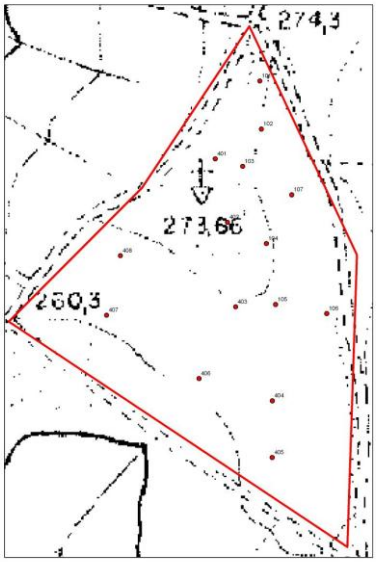

Figure 46 :Topographic map of the study area with location of soil samples.

Grain size of the selected parcel (Figure 46) generally corresponds to silty sand. From the pedologic point of view, the soil in the selected parcel shows a muddy texture and a coarse prismatic framework. It is wide, not very deep and not well drained. The landscape is dominated by several hills subjected by both intense massive and superficial erosive processes. The regolith is represented by lacustrine mud with intercalations of cohesive and reddish silty layers. Vermiculite and montmorillonite have been detected within the lacustrine mud. This soil shows widespread cracks, up to 4 cm deep, developed during the dry season.

3.1.2. Validation database

The studied area was separated into two parts (see black lines on Figure 47) presenting two different crop operations: 1) at the top the soil was no tilled, 2) the rest of the field was ploughed and presented a strong surface roughness. A topographic map was realised by a precise DGPS installed in the ARP system. 29 locations were georeferenced for the validation database.

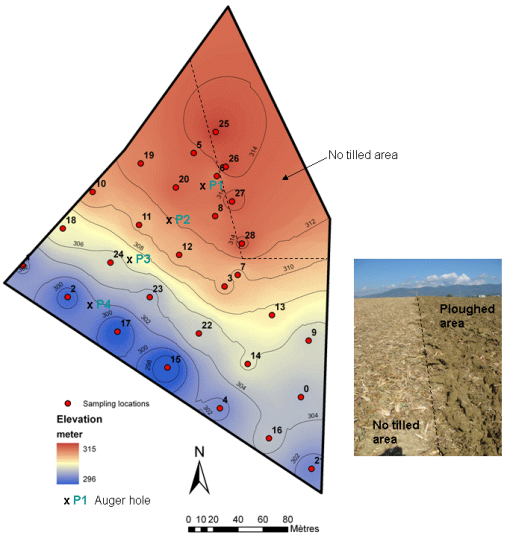

Figure 47 : Topographic map with sampling locations; The black line present the limit between tilled and no tilled area. The cross are locations of auge holes for the pedologic description.

The topography shows a relative important change in altitude: 14 m between the top and the bottom of the studied area.

29 cylinders were sampled (see locations on Figure 47) for the validation database. We used 85 mm diameters and 90 mm height cylinders (Figure 48).

Figure 48 : Cylinders used for sampling

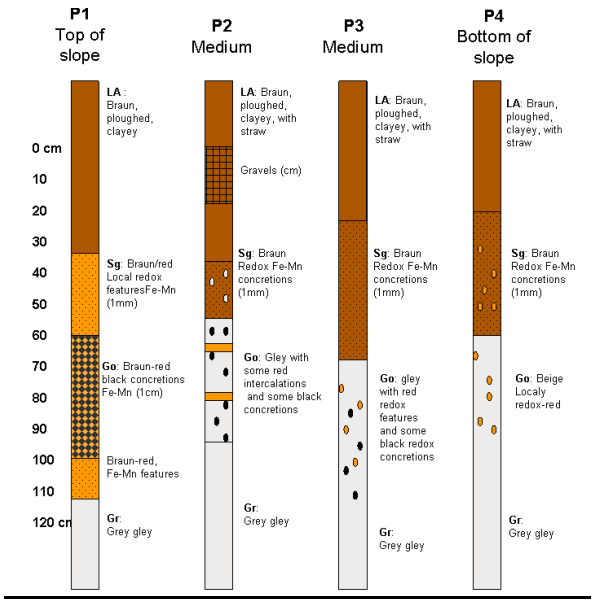

Figure 49 : Pedologic description from auger holes

The soil description shows a high level of clay content for surface horizons whatever the location. Local hydromorphies (Fe-Mn) can be observed in these horizons. A Gr horizon (Grey gley) was detected at variable depths (between 50 and 110 cm). This formation is link to oxidation and reduction processes du to water level variations. An hypodermic flow over the Grey gley is highly possible during wet periods due to the high level of clay content.

Four augers holes (P1 to P4, Figure 47) were realized along the main direction of the field slope. *Figure 49* presents schemes of the different horizons observed.

- The observed C content map:

The SOC content was measured in the plough layer, and in 10 bare fields within the flight lines of the SIMGA sensor (Figure 50)

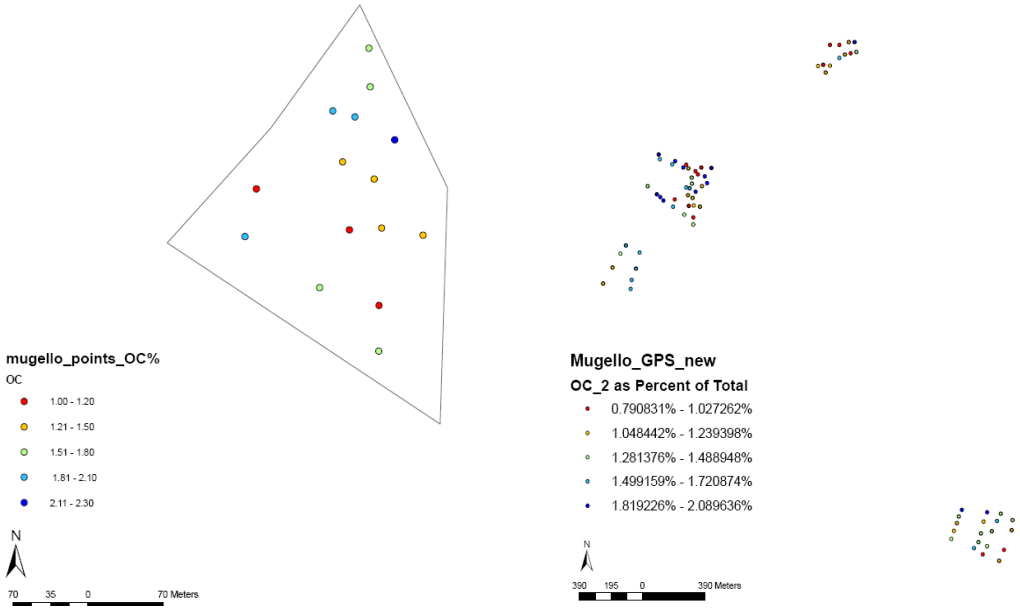

Figure 50 : SOC measured data.

- Observed water content

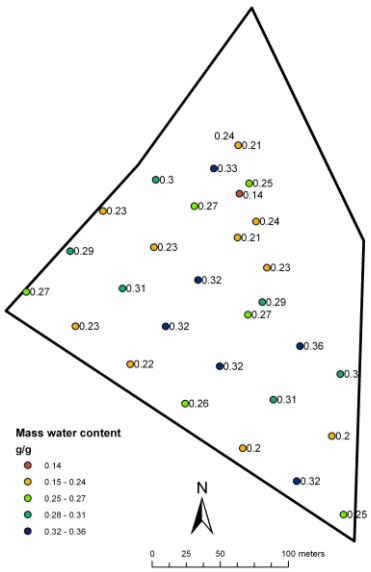

Figure 51 : Mass water content at 20 cm depth

The mass water content was measured directly in the fine earth from the soil cores (Figure 51) at 20 cm depth.

The water content analysis in the surface horizon exhibit values from 0.2 g.g-1 to 0.35 g.g-1. It can be observed a spatial organisation: low values at the bottom of the field and high values in middle part of the field. This can be explained by a slope effect combined with layering of the soil. Values in the no tilled area (top of the field) present relatively low values probably link to a structure effect.

- Observed soil bulk density

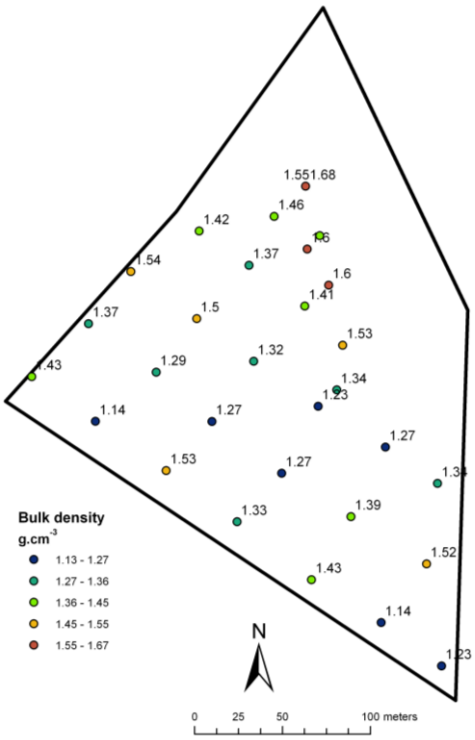

Figure 52 : Soil bulk density at 20 cm depth

The bulk density was measured directly in the fine earth from the soil cores (Figure 52) at 20 cm depth.

There is a strong difference in bulk density between the two crop sytems (ploughed and no tilled): bulk densities in the no tilled area are equal to approximately 1.6 g.cm-3 whereas in the rest of the field, values are comprised between 1.15 and 1.5 g.cm-3. The ploughing is responsible for an increasing soil macroporosity.

- Observed Clay content

Traditional laboratory analysis (Rietveld XRD determination of clay content) on collected soil samples results an IDW interpolated clay content map as basis for the validation of total Clay map from Hyperspectral images (Figure 53**).**

3.2. GEOPHYSICAL MEASUREMENTS REALIZED

3.2.1. Geoelectric

- Measurement report

Electrical resistivity measurements were obtained at the field scale by the use of the ARP device (see part 2.2.1). The measurements were realized along transects separated by 1 m covering the entire studied field. Along one transect, measurements were performed and recorded every 10 cm.

Sample	*T.Clay*
M01-03	41.02
M01-05	57.13
M01-06	63.09
M01-07	55.53
M02-01	64.44
M02-03	51.32
M02-05	41.53
M02-07	46.03
M03-01	63.98
M03-02	53.67
M03-03	36.73
M03-04	50.31
M03-05	51.81
M03-06	56.23
M03-07	64.02
M04-01	46.83
M04-02	46.07
M04-03	56.80
M04-04	53.94
M04-05	64.80
M04-06	60.61
M04-07	54.52
M04-08	61.19
M05-03	49.69
M05-04	49.95

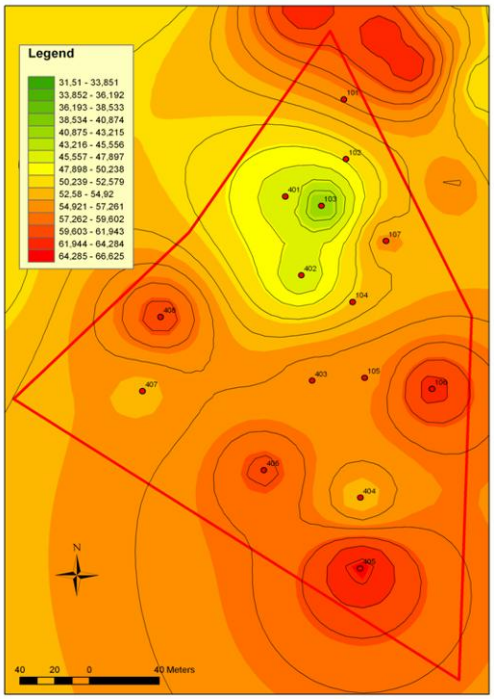

Figure 53 : IDW interpolated map of soil Total Clay content as results from laboratory analyses.

Local 2D and 3D Electrical resistivity Tomographies were realized…

- Timetable and human effort: The electrical measurements were run on the field by one operator during one day.

- Processing: The ARP raw data have been filtered by 9 median filters. The value of one data is replaced by the value of the median of the 9 values around if it is different of 40%.

- Geophysical map

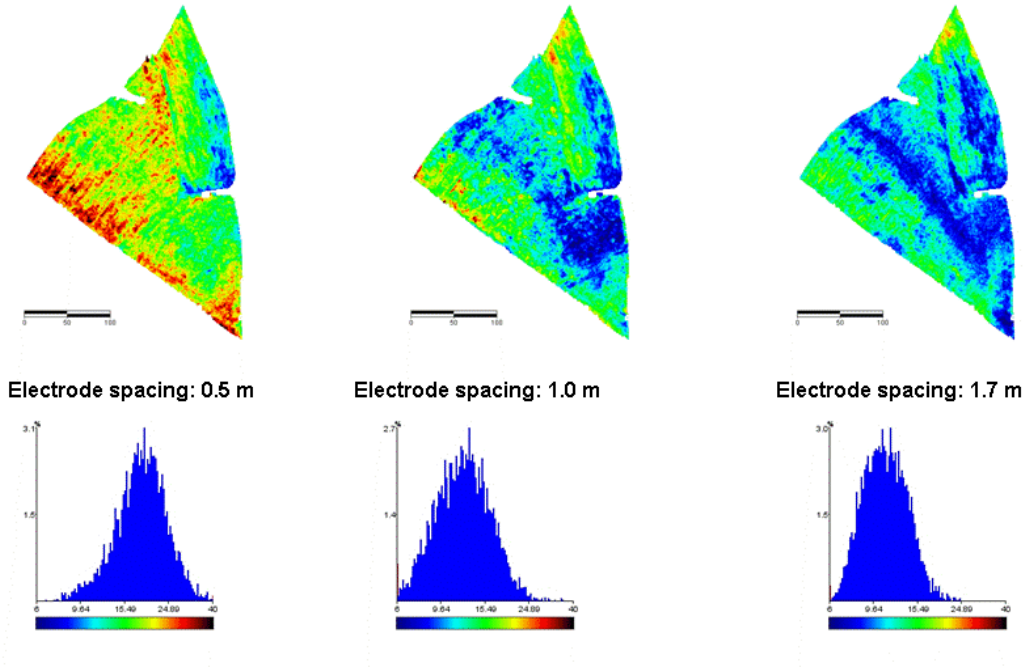

Figure 54 :ARP results for the 3 investigation depths

The electrical resistivity map presents relatively low resistivity values: from 5 to 40 ohm.m due to the high clay content. The higher the investigated volume, the lower the resistivity. This can be explained by the high content of clay in the soil which increases from surface to deep layers (see pedological description previously).

For the first investigation depth, the resistivity values are lower in the no-tilled area. This could be explained by the combined effect of hydric (lower water content) and structural properties (higher bulk density).

In the middle part of the slope, the resistivity values are lower for the two last electrode spacings. This is consistent with spatial distribution of the water content.

3.2.2. Seismic

- Measurement report

Seismic experiments on Luxembourg site led to realize 10 profiles covering few ha for almost 300 seismic shots. In addition, 10 penetrometers were performed on the same area to validate the method.

  - Location map of measurements

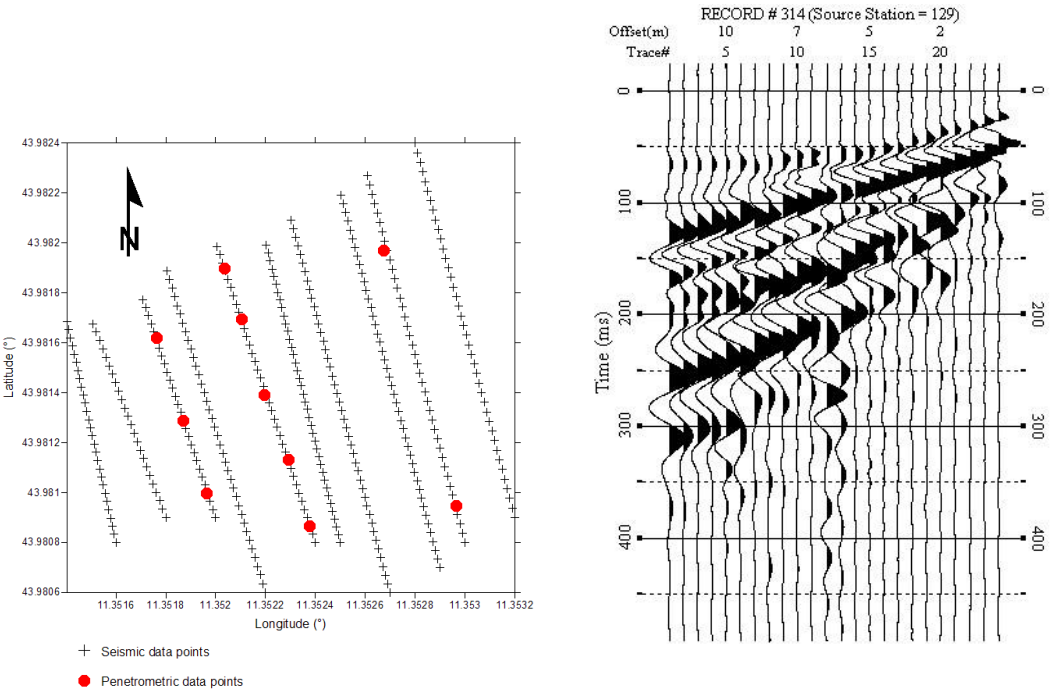

Figure 55 : Location map of seismic and penetrometer acquisition points over the Mugello site (left). Example of a seismic shot.

- Timetable and human effort: The Digisoil's seismic system was run on the field by two operators during two days; another day was dedicated to penetrometry measurements and trench observations.

- Processing: A traditional SASW processing flow was carried out on thios dataset, involving: Rayleigh wave dispersion diagrams computation for each seismic shot, dispersion curve picking, Vs inversion, 2D interpolation along 2D profiles. Then, by analyzing a statistic multimodal velocity distribution, the velocity value corresponding to the limit between the soil and the mechanical bedrock is estimated and validated with the penetrometry data and trench observations.

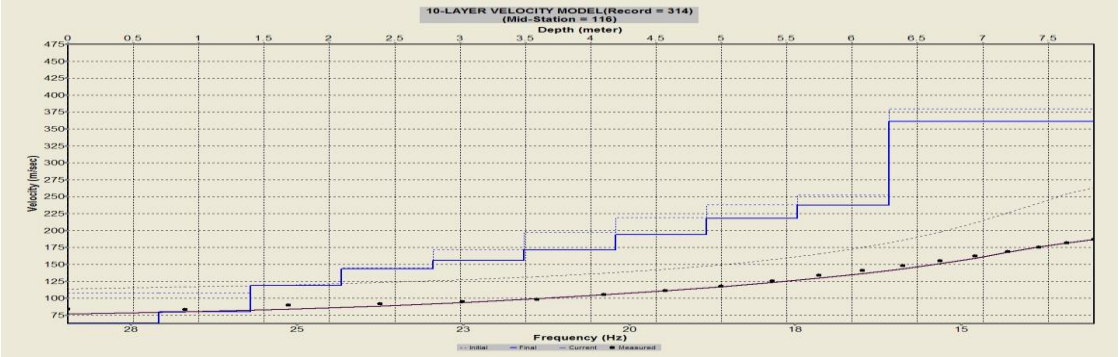

Figure 56 : Observed dispersion picks (dot), computed dispersion curve (red line) and inverted velocity profile (blue line).

- Presentation of the geophysical maps

The geophysical map was derived from the interpolation of 2D Vp tomograms obtained after P-wave first arrivals inversion.

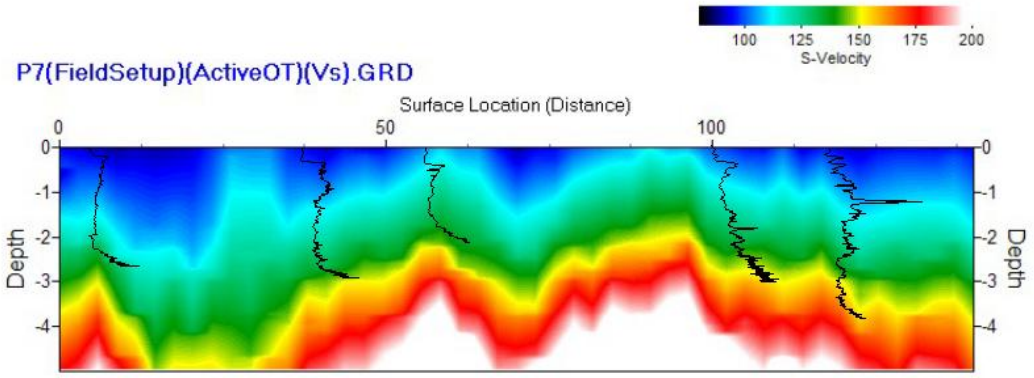

Figure 57 : exemple of 2D Vs section after inversion of Rayleigh wave dispersion. The black lines represent the penetrometry data.

When interpolating all the dataset in a 3D velocity model, a map of the soil depth and soil velocity can be derived. These maps can be afterwards compared to the validation dataset, i.e., penetrometry, to estimate the a posteriori uncertainty related to the method.

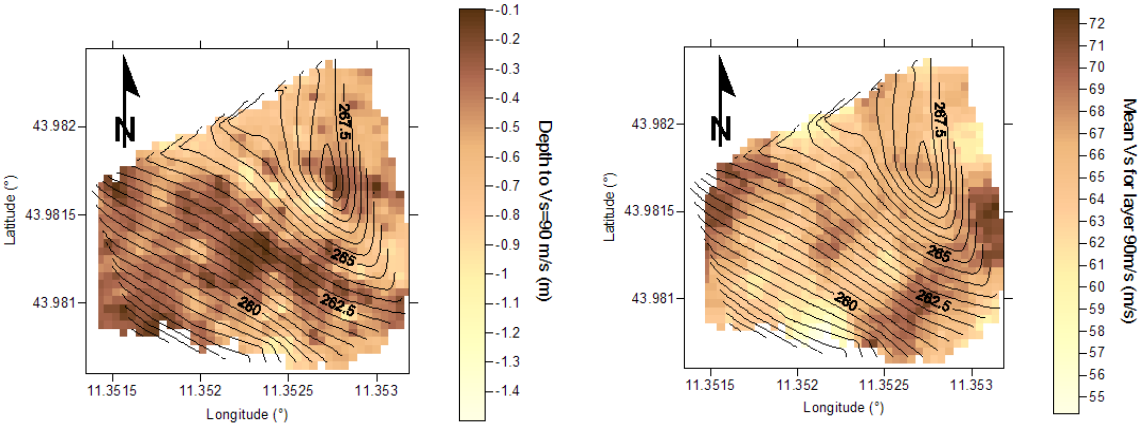

Figure 58 : Maps of soil depth (left) and Vs values (right) over the Mugello site.

- Spatial structure and data interpolation

The spatial structures of the soil depth was assessed from variograms estimated along four directions: 0°, 35°, 90° and 135° from geographic north. The variograms were generated from all possible sample pairs in a given direction grouped into classes (lags) of approximately equal distance (Matheron, 1965). The variance (one-half of the mean squared difference) of the paired sample measurements were then plotted as a function of the distance between the samples to provide a means of quantifying the spatial structure of the data. The soil depth obtained using seismic method was then interpolated by ordinary kriging - a geostatistical method that takes into account both the distance and the degree of variation between known data points and relies on the data's spatial correlation structure to determine the weighting values. Ordinary kriging has been shown to perform better for soil parameters than other available methods (e.g. Burgess et al., 1981; Myers, 1994). The interpolations were accomplished by fitting each of the various theoretical variogram models to the empirical isotropic variogram via the least-square method (Figure below). The best fit model was used for the interpolation. Data points were then interpolated to a regular grid using a full second-order polynomial drift function, as is common practice. With the interpolation process, we then create an output grid of kriging standard deviations which brings information about the interpolation error. The figure below shows that the minimum interpolation error for the soil depth to Vs=90m/s (between 0.02 and 0.2m) is situated at the location of data points and the maximum interpolation error (between 0.2 and 0.3m) is located between data points; In the same way, the minimum interpolation error for the mean Vs to Vs=90m/s (between 1 and 5m/s) is situated at the location of data points and the maximum interpolation error (between 5 and 9m/s) is located between data points.

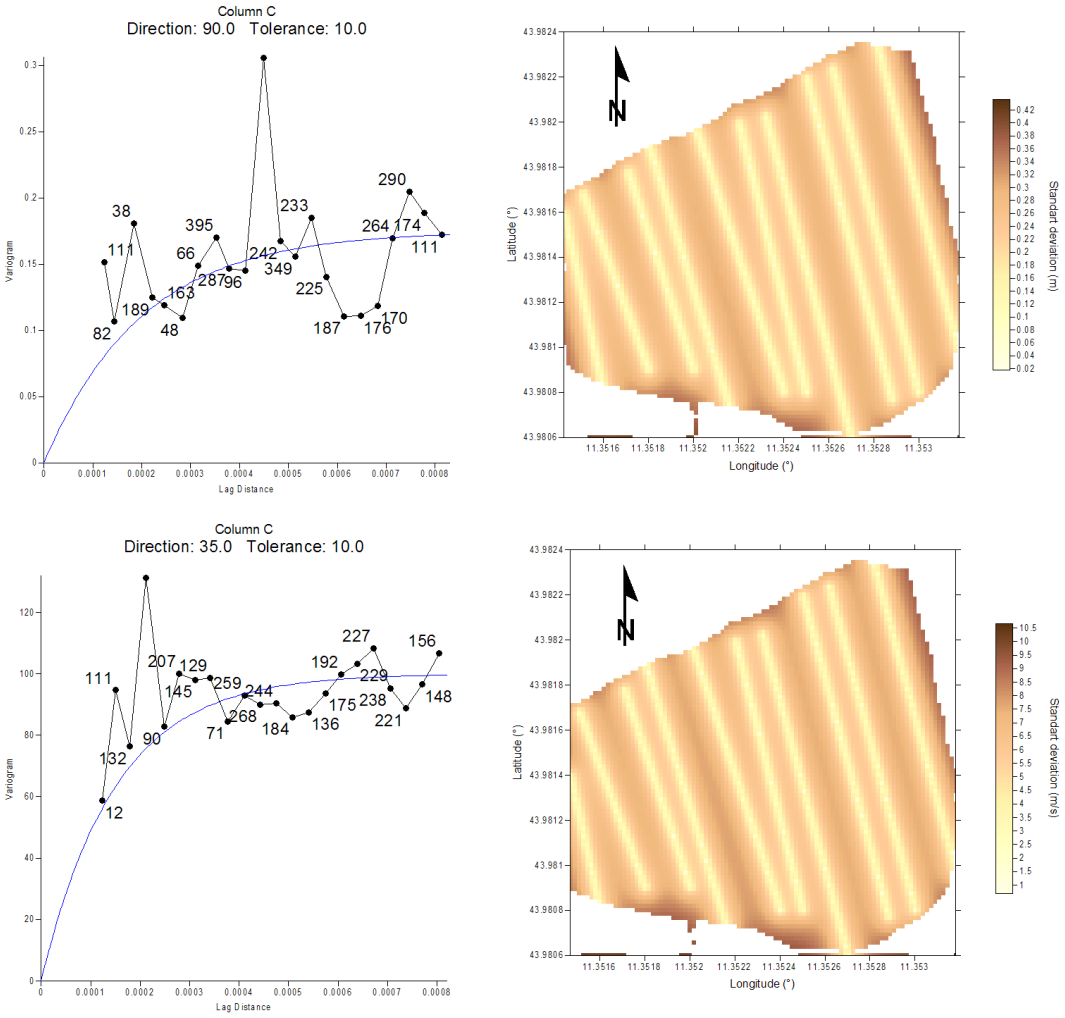

Figure 59 : (Left) Example of a vaiograms estimated in the direction 90° (Top) and 35° (Bottom) from geographic north for the Vs=90m/s case. Variograms are fitted with a theoritical variogram model using (Top) an exponential component with scale=0.175, Length=0.0002, anisotropy ratio=1.157 and anisotropy angle=84.82° and (Bottom) an exponential component with scale=100, Length=0.00015, anisotropy ratio=1 and anisotropy angle=0°, (Right) kriging standart deviation maps.

3.2.3. Hyperspectral

On September 23rd-24th 2009, a complete hyperspectral geocoded reflectance dataset was collected using SIM.GA hyperspectral image sensor from Selex-Galileo (Figure 60), mounted on board of the University of Florence ultra light aircraft (Figure 61). The approximate pixel resolution was 0.6 m (VNIR) and 1.2 m (SWIR), considering a height of flight of about 900 m. The flight plan, as well as the sampling strategy, were defined on the basis of a preliminary survey to identify the bare soil fields available in the scheduled period. Available pedologic, geologic and geomorphologic maps were also examined. Seasonal agricultural

activity influenced the period chosen for field experiments; in fact, since the hyperspectral technique needs bare terrains to produce a prediction of soil properties, the scheduled period for field analyses was the second half of September, when most of the parcels are ploughed and milled. Soil samples (to a maximum depth of 5 cm) were collected (positions recorded with a Leica 1200 differential GPS) simultaneously with the flight of SIM.GA hyperspectral camera and underwent traditional laboratory analyses (Rietveld XRD determination of clay content) and laboratory spectral signatures collection under controlled conditions, using an ASD FieldSpec spectroradiometer, provided with an illuminating device with stabilized krypton lamps, with fixed viewing and shooting geometry.

SIM.GA technical specifications	VNIR	SWIR
spectral range	400-1000 nm	1000-2500 nm
spectral sampling	1.2 nm	6.3 nm
# spectral pixels	500	256
IFOV per pixel	0.7 mrad	1.3 mrad
digital resolution	12 bits	14 bits

Figure 60 : Hyperspectral SIM.GA sensor technical specifications

Figure 61 : SIM.GA camera mounted on board of UNIFI ultralight aircraft.

The ASD spectroradiometer (Figure 62) was used during flight as well, for ground measurements aimed at the characterization of atmospheric conditions (solar radiance and irradiance) and for reflectance measurements on reference targets such as metal panels and pcv sheets (Figure 63).

ASD FieldSpec technical specifications	
FOV	25°
spectral range	350-2500 nm
spectral resolution	3-10 nm
# bands	2151
sampling interval	1.4 nm (350-1000 nm) and 2 nm (1000-2500 nm)
frequency of acquisition	10 spectra/sec

Figure 62 : ASD FieldSpec technical specifications.

Figure 63 : Field measurements with ASD FieldSpec on soils (a) and reference targets (b, c).

Figure 64 shows the IDW interpolated map of total clay content, as well as the correlation between clay content and the absorption peak depth at 2200 nm and between clay content and the ASD “Bierwith” (Kanlinowski & Oliver, 2004) band ratio.

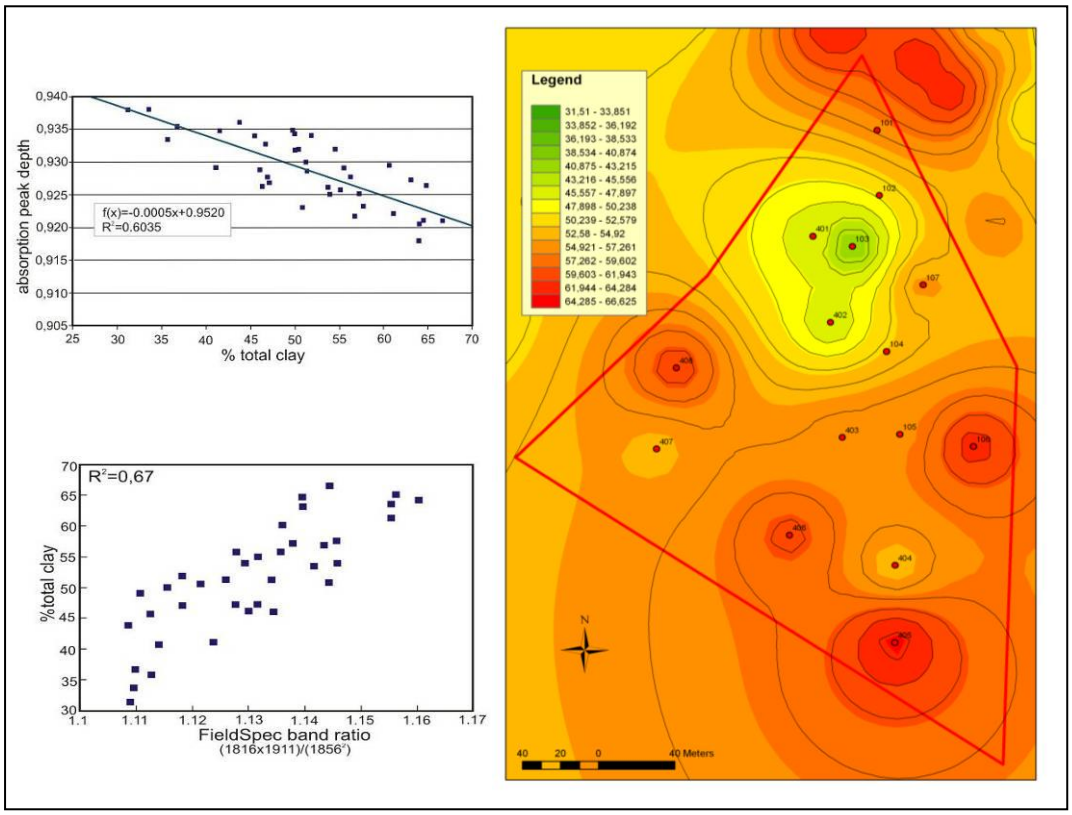

Figure 64 : Interpolated map of clay content values for the selected study parcel.

A dedicated photogrammetric aerial survey was performed by UNIFI to obtain a 0.5 m precision digital elevation model, for orthorectification of SIM.GA images. The aero photogrammetric survey has been developed according to the following phases:

1) definition of the photogrammetric flight project for the development of three-dimensional optical models, with a suitable scale for the implementation of a regular grid DTM. After determining the appropriate photographic scale and retrieving the proper flight altitude, taking into account the focal width of the camera, the shooting was designed in order to cover the same surface of each strip as covered with SIM-GA; then, the coordinates of the ends of the flight strips were calculated and the relative orientations of the flight paths were obtained, in order to assist the navigation through the GPS system.

2) Frames acquisition. The frames were acquired with the UNIFI Groppo Folder aircraft, using a Nikon D700 digital camera with calibrated focus. The internal orientation parameters (main point, focal distance, radial lens distortion, pixel size) were previously determined in laboratory and processed with the stereo photogrammetric Micromap Work Station - GEOIN.

3) Choice of the frames suitable for yield. Since all the frames were acquired with a field longitudinal overlap of about 80%, the number of frames actually used for realizing the models was less than 50% of the total acquired.

4) Definition of the ancillary survey with GPS for absolute orientation of stereograms. The topographic survey campaign, aimed at the determination of points required to determine the absolute orientation of each model, was conducted using three GPS stations at the same time. The coordinates of about 50 homogeneously distributed points inside every single flight strip were registered (Figure 65).

Figure 65 : Ancillary GPS survey for orientation of the stereograms.

5) Final product. After the necessary aerial triangulation for the metric placement of the stereoscopic models, the DTM strips were obtained with the digital stereo photogrammetric work station Micromap - GEOIN. The collected data were enough to describe the ground morphology with a grid of 2m x 2m (0.5 m altimetry precision) as required by Galileo for SIM.GA hypercubes. The altimetric data of woody, bushes and built areas were removed from the DTM. The final product in CAD vector format was finally transformed in shape format in order to facilitate any subsequent processing activity.

Total time spent on the field by the UNIFI team was three days for the sampling/spectral signature collection campaign, plus two-three days for preliminary field survey.

- Processing

The full processing chain of Hyperspectral SIMGA data was performed by GAV team which provided geometrically and atmospherically corrected at-surface reflectance data. A parametric geocoding correction was performed on the basis of flight attitude and GPS sensor position data collected by the Inertial Motion Unit IMU co-aligned inside the sensor over a digital elevation model.

On the basis of FieldSpec measurements a spectral index based on 2210 nm absorption of clays was derived and a linear relationship with total clay contents from laboratory analysis was found for the inversion of the same clay index based on airborne Hyperspectral data. (Figure 64). The resulted total clay map is shown in Figure 66 to be compared with the IDW interpolated map for validation.

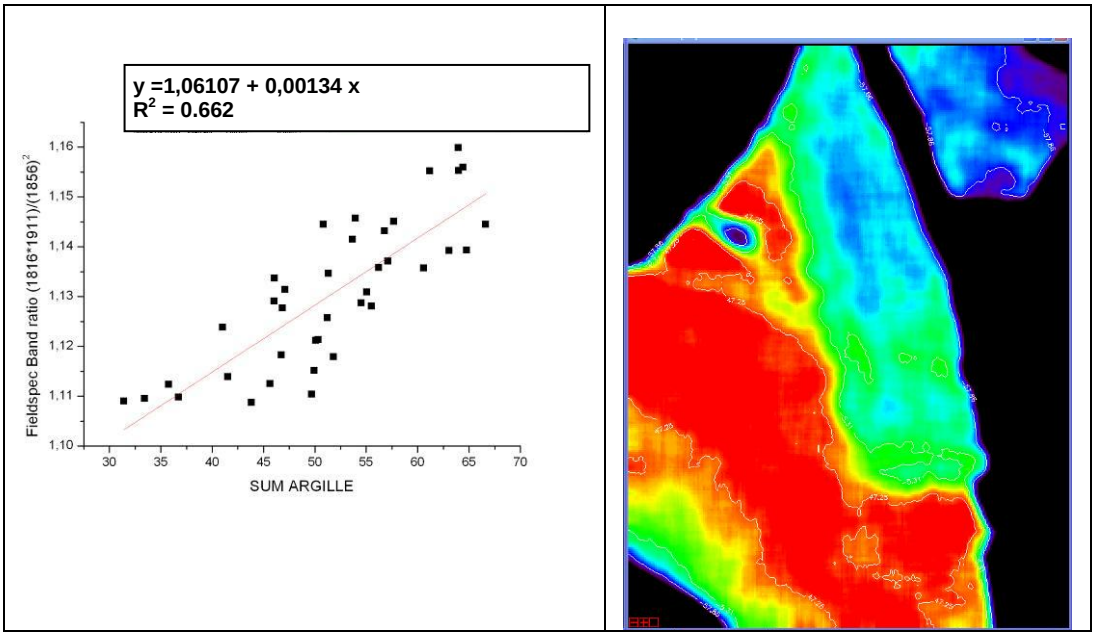

Figure 66 : a) Experimental relationship between spectral measurement and cly content; b) Total clay map from airborne hyperspectral data.

- Timetable and human effort

UNIFI team: Total time spent on the field by the was three days for the sampling/spectral signature collection campaign, plus two-three days for preliminary field survey. Airborne transects acquisition required about 1 hour of flight.

GAV team: for the airborne campaign three persons were employed for sensor installation and start-up, radio link with airborne, spectral ground measurement on calibration targets (painted metal panels and white PVC sheet). We consider to spend one week (one person) for the full data correction and processing up to the retrieval of the Clay content map.

3.2.4. EMI

- Measurement report

For the Mugello site, the EMI setup was identical as that used in Luxembourg, namely, the EMP-400 Profiler (GSSI) instrument operating at three frequencies

(5, 10 and 15 kHz) carried by the operator during the measurements, and the EM38 sensor mounted on a quad together with the GPR system. The data were geo-referenced using a differential GPS.

- Location map of measurements

As for Luxembourg, EMI measurements were carried out along transects spaced approximately 10-15 m apart, with about 1 m resolution within the transects. Data were acquired simultaneously with the EM38 in vertical dipole orientation and with the Profiler in horizontal dipole mode on the 29th September 2010, and vertical dipole Profiler measurements were performed on the 30th September 2010. On the first day, data were collected all over the studied area, while the north-east part of the field was inaccessible on the second day because of soil tillage in progress (Figure 67).

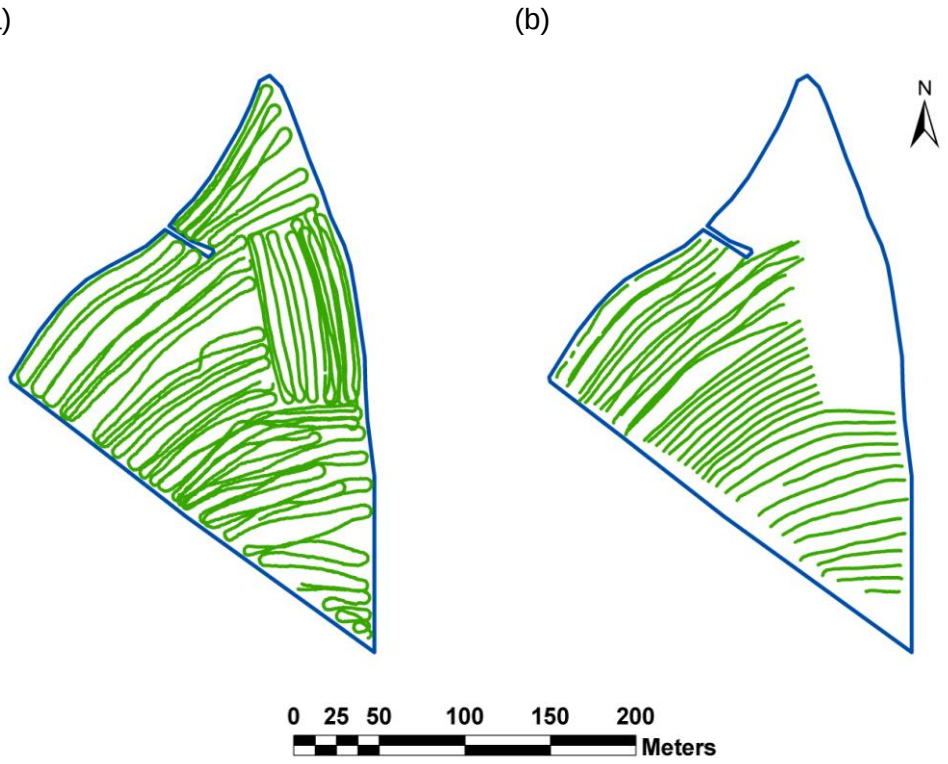

Figure 67 : Location of the EMI measurements in Mugello with (a) EM38 in vertical dipole and Profiler in horizontal dipole modes (29th September) and with (b) Profiler in vertical dipole orientation (30th September).

- Timetable and human effort: On 29th September, around 7 hours were necessary for two operators (one person in charge of the Profiler, the other one driving the quad equipped with the EM38 and the GPR) to collect the data over the total area (~5.5 ha). On 30th September, one person performed the Profiler vertical dipole measurements during

about 5 hours over the restricted area (~4 ha). The much lower time efficiency for the measurements over this site by comparison with the Luxembourg site results from the hard field conditions for measurements, due to both the steep slope and the very high roughness of the soil surface which was freshly ploughed.

- Processing: As for the Luxembourg site, the soil apparent electrical conductivity values provided by the sensors were standardized according to the reference temperature of 25°C using the equation proposed by Sheets and Hendrickx (1995). At this site, the average soil temperature during the measurements was 19.1°C.

- Geophysical map

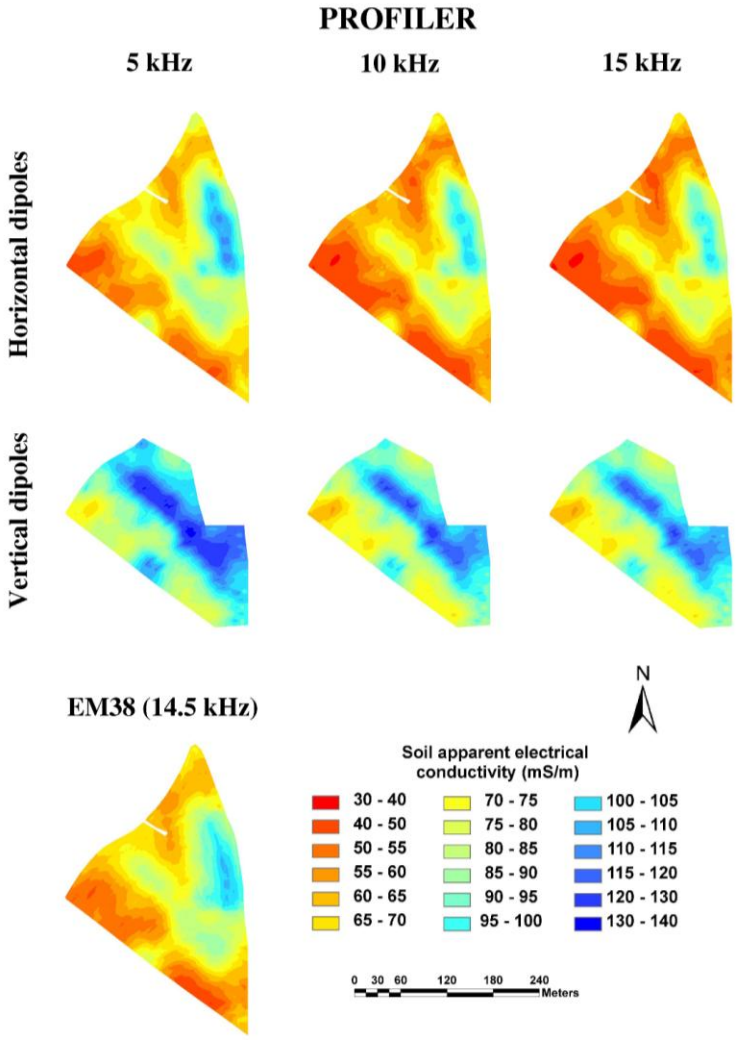

Figure 68 : Maps of the soil apparent electrical conductivity measurements performed with the EMP-400 Profiler and EM38 sensors over the Luxembourg site.

The interpolated maps of soil electrical conductivity measurements performed at the Mugello site with both sensors are presented in Figure 68. At this site, values of soil electrical conductivity are much higher (30-140 mS/m) than those observed for the Luxembourg site (< 20 mS/m). Moreover, the spatial variations of soil electrical conductivity are also much more pronounced. Looking at the Profiler horizontal dipole measurements, we observe very high conductivity values over the no tilled area, intermediate values in the middle part of the field (where the slope is the steepest, and lower values at the bottom of the field. Similar spatial patterns of soil electrical conductivity are observed for vertical dipole mode measurements, but with much higher values compared with horizontal dipoles. These spatial patterns correspond well to that of ERT data. For both horizontal and vertical data sets, soil electrical conductivity tends to decrease slightly as the frequency increases. For EM38, the spatial patterns of soil electrical conductivity are similar to that observed for Profiler. Moreover, though measurements with EM38 were performed with vertical dipole orientation, the soil electrical conductivity values obtained with this instrument are within the range of values found for Profiler in horizontal dipole mode. Differences between both instruments for the antenna offset (EM38: 1 m, Profiler: 1.22 m) and the antenna height above the soil surface (EM38: 0.4 m, Profiler: 0.2 m) may at least partly explain these observations, as these two parameters affect the investigation depth. In other respects, as aforementioned for the measurements in Luxembourg, a part of the differences in absolute values of soil electrical conductivity observed between the data sets may arise from the lack of robustness of sensor calibration.

3.2.5. GPR

3.2.5.1 Off-ground GPR

As for Luxembourg, the combination of a Vector Network Analyzer (VNA) and a horn antenna (200-2000 MHz) located at 1.1 m height, was used to perform the off-ground measurements. The system was mounted on a quad and a differential GPS was used for data geo-referencing. The data acquisition was controlled by a portable computer which recorded measurements every 1 second.

- Measurement report
    - Location map of measurements

The off-ground GPR measurements were performed all over the studied area at the same locations as the EM38 measurements.

- Timetable and human effort: The velocity of the off-ground GPR system along the transects at the Mugello site was less than 0.5 m/s because of the high surface roughness and field conditions. Therefore, the complete off-ground measurements took around 7 hours for one person.

- Processing:

GPR data were inverted using the model of Lambot et al. (2004, 2006) by focusing on the surface reflection, as fully documented in Grandjean et al. (2009) (section 3.2.1). Because of the high roughness of the soil surface over most of the field area, we selected the range of frequencies lower than 650 MHz for processing, which provided the best fitting of the model to the data. The retrieved dielectric permittivity is shown in Figure 69 using kriging interpolation.

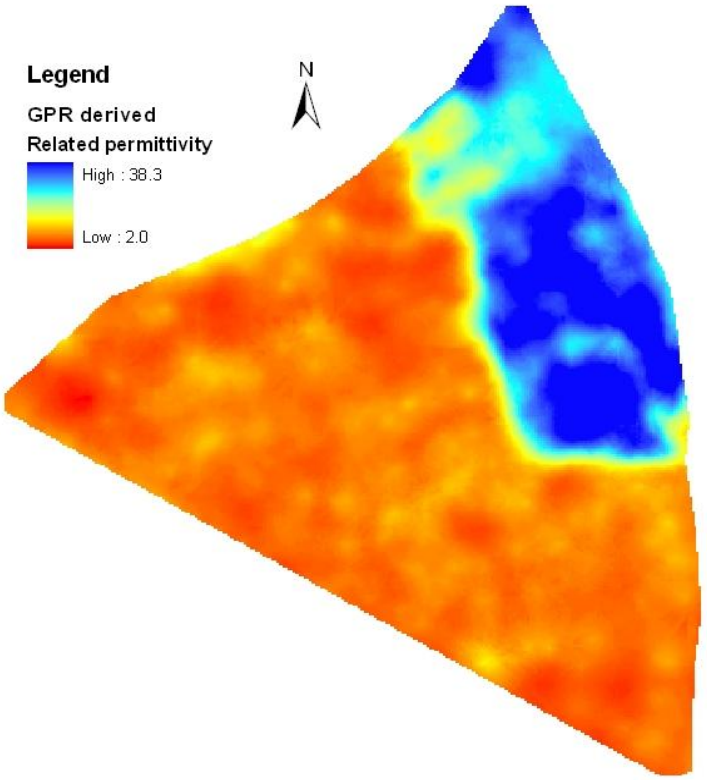

Figure 69 : Relative dielectric permittivityof the shallow soil retrieved from off-ground data inversion at the Mugello site.

3.2.5.2 On-ground GPR

As for Luxembourg, we used a time-domain GPR system (model SIR-20, Geophysical Survey System, Inc., GSSI, Salem, Massachusetts, USA) combined with a pair of 400 MHz shielded bow-tie antenna located at 1.1 m distance from each other as an impulse radar. Applying the two antennas helped us to use the monostatic and bistatic modes simultaneously.

- Measurement report
  - Location map of measurements

The on-ground GPR transects correspond to those followed for the Profiler in vertical dipole orientation mode.

- Timetable and human effort: As for the off-ground survey, on-ground GPR measurements were performed at a velocity of about 0.5 m/s, using 1 person for driving and controlling the system. Around 5 hours were necessary for the field campaign.

- Processing: A gain function (power gain function of time with factor varying between 1-3.5) was applied for better visualizing the GPR signal in the radargrams. Processing the on-ground GPR data showed no information for qualitative interpretation of the radargrams. The only reflection that was visible in the radargrams was the surface reflection, which contains information related to the water content. However, the high soil surface roughness at the study site makes the processing of these data impossible. As an illustration, Figure 70 presents one of the on-ground GPR transects performed in Mugello.

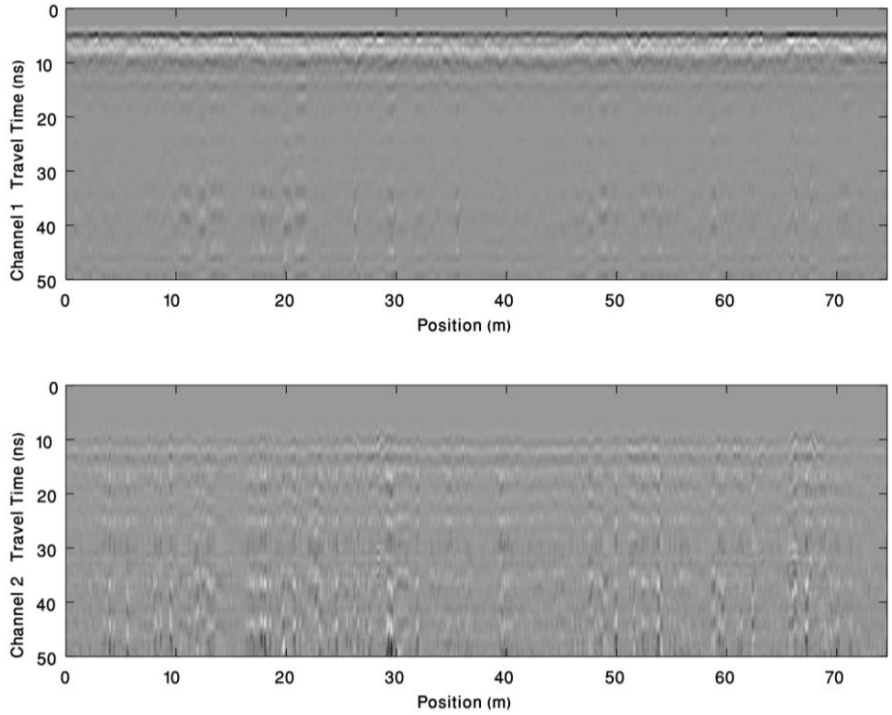

Figure 70 : Transect 35 of on-ground GPR survey in Mugello,with both monostatic and bistatic radargrams.

- Water content map

Using the off-ground imaging and inversion by means of Lambot et al. (2004, 2006) model focusing on the surface reflection allowed to retrieve the dielectric permittivity of the shallow soil. Based on these estimates, the Topp (1980)

equation was then used to determine the corresponding soil water content. Figure 71 presents kriged water content for the entire field. High water content values are observed for the no tilled area of the field, while much lower water content estimates are found over the ploughed area. It is worth noting that a part of these differences may arise from the very high roughness of the soil surface over the ploughed area. Indeed, though we selected the lowest frequencies for data processing, such field conditions affect the GPR measurements and the derived water content estimates. In particular, roughness decreases the amplitude of the surface reflection due to scattering and, hence, leads to significant underestimations for the surface dielectric permittivity and correlated water content. This can be observed in Figure 72 where the dielectric permittivity is significantly underestimated compared to the ground truth measurements assuming Topp's model as petrophysical relationship. We therefore conclude that due to too large roughness at this test site (amplitude larger than 25 cm!), it was not possible to estimate water content using off-ground GPR with frequencies larger than 200 MHz.

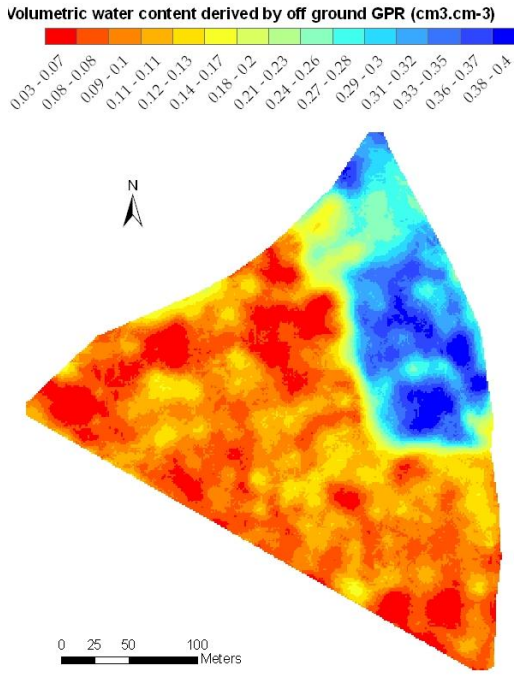

Figure 71 : Water content estimates from off-ground GPR measurements at the Mugello site

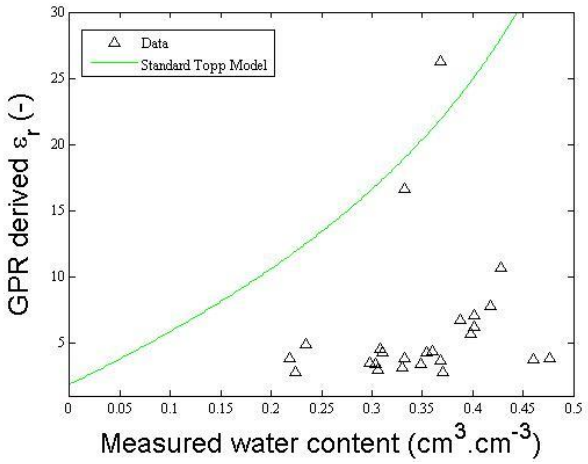

Figure 72 : GPR-derived dielectric permittivity as a function of ground-truth volumetric water content at the Mugello site

4. Zala site

4.1. SITE LOCALISATION AND PRESENTATION

For the Zala site a large database exists that covers a large area of cultivated fields (about 10 000 ha total). On each of these fields a point was sampled (kind of soil, water content, pF, etc.). From these sampled locations, a detailed soil map can be constructed (Figure 73).

But the sampled points lie at least about a 100 m and at most 400 m apart. Consequently it can be difficult to infer exact limits and their geometry between the different soil units using only geo-statistical tools. In such a case, the use of geophysical mapping and /or profiling is highly interesting, provided the geophysical measurements can yield information that is relevant for inferring soil properties that are of interest for agricultural needs.

Detailed resistivity (and IP) measurements along fixed lines in 2D or 3D are what can be provided using the Abem TerrameterLS and small electrode spacing of 0.5 m or even 0.25 m. Such small spacing is necessary to obtain a good resolution over the agricultural soil (down to max 1.5 m), but they imply slow progress over the area, since many electrode positions are to be considered. It is therefore impossible to measure over the whole area, or even to perform exhaustive mapping of even one field using that method within a reasonable time. As an example, detailed measurements with such spacing take about a day for a 150 m long profile. On the other hand, they can provide detailed information about the different soil horizons, their geometry and composition, and properties like water content and permeability (or capacity to retain water and have it available for crops, like is measured by the pF).

Therefore, we chose to measure resistivity and IP over one long profile over an accessible field and to complement the geophysical measurements with soil sampling performed just afterwards, so as to provide an assessment of the relevant soil information that can be obtained that way at this site. This profile was even completed by a small perpendicular profile including the only point previously sampled and recorded in the database. The results can most likely be used and referred to if, and when, a more extensive geophysical should be undertaken.

The chosen field lay in fallow this year. It is situated on the side on a small hill, and for that reason changes in soil properties were expected related to topography.

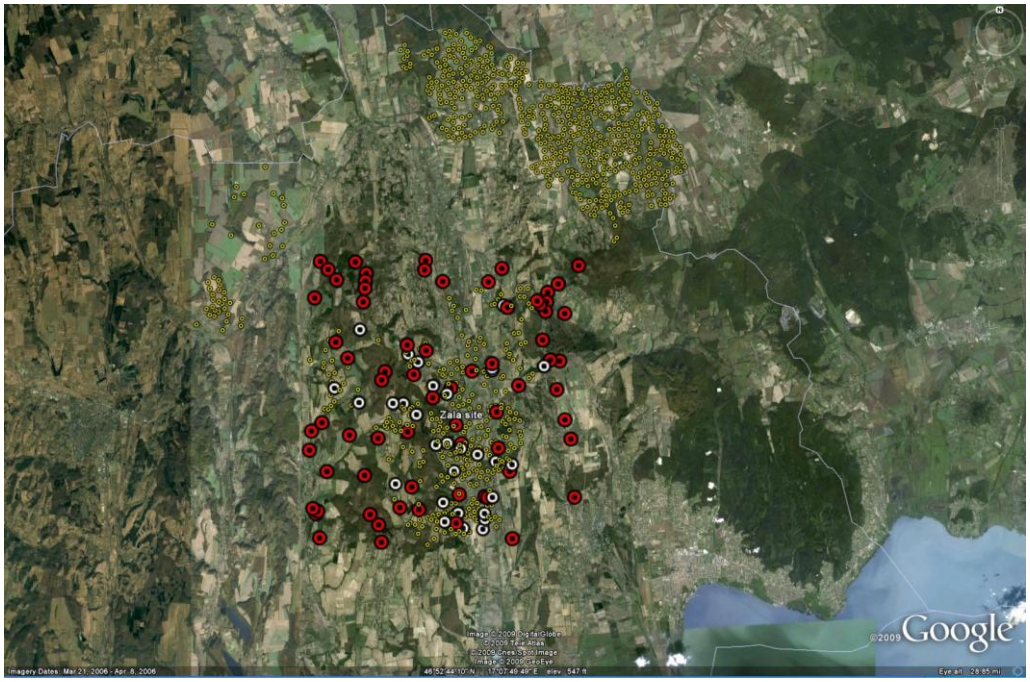

Figure 73 : Zala site location with ground truth samples posting

4.2. WATER CONTENT MAP VARIATIONS

- Specific remarks

Soil horizons and composition, as well as their pF (or measure of their capacity to retain water) are stable properties over several years. Water content on the other hand, as well as temperature, is highly variable, depending on the season and meteorological conditions. Resistivity will show changes related to these two variable properties, even if it is also related to the first, more stable ones. Therefore, one measurement is bounded to one time occurrence.

Induced polarization can probably be better related to soil capacity to retain water since the surface conduction it depends on is specifically related to pore size distribution and geometry. However the relationship is complex and likely to depend on the specific material considered. Spectral information can be obtained from time-domain measurements like the ones we have performed, but with a limited bandwidth, depending on the technique used and on the noise level. Induced polarization is in general more difficult to measure compared with resistivity, because the electrical potentials involved are small, often much smaller than the ones due to other causes.

Measurements with small electrode spacing require more accurate positioning than “usual”. It is not always easy to obtain on a rough agricultural surface. With a differential GPS we can expect an accuracy of about 2 cm, which is about 4% for 50 cm spacing, and 8% in case 25 cm spacing is used. About the same accuracy

can be reached using measuring tapes laid on the ground, but errors can be cumulated and it can be time consuming. For that reason, and because it is relatively simple to use, every other electrode was positioned with a differential GPS.

- Geoelectric line location

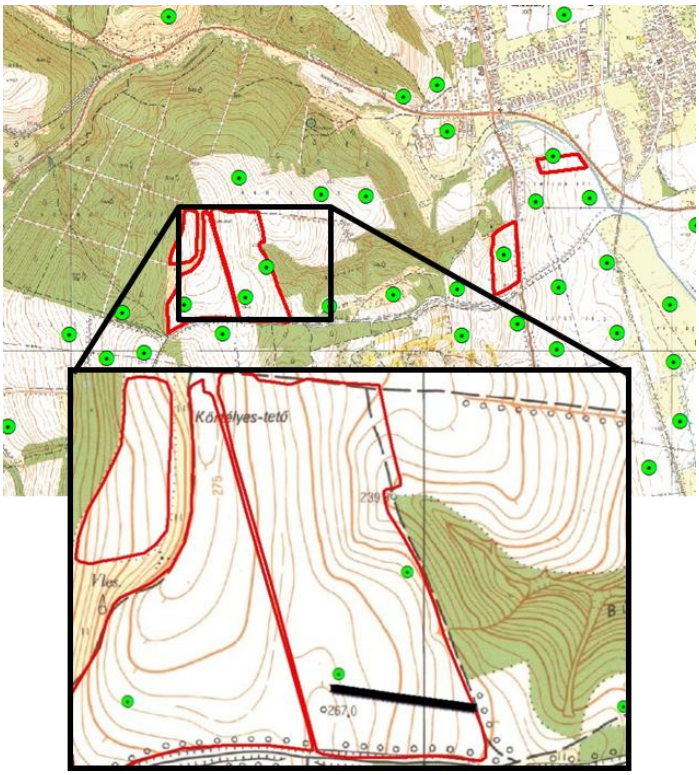

Figure 74 : Geoelectric line location map on the Zala site

- Measurements and interpretation

Resistivity and IP were measured using the Abem TerrameterLS, two multicore cables with 32 take-outs each designed for 50 cm spacing and steel electrodes. The electrodes were pushed only about 5 cm in the soil so that they should remain small relatively to the other distances. It has been shown that stainless steel electrodes can be used even for induced polarization measurements, provided the “natural” potential at the electrodes is almost stable and accounted for. The Terrameter LS used alone can handle 64 electrodes at a time. It is a 12-channel instrument and it records the potential curve at the potential electrodes with 1 ms sampling interval, as well as the current and potential sent at the current electrodes with the same sampling interval. It also records the contact resistances at all the electrodes.

Here we have used a 4 s 50% duty cycle, and a maximum current of 50 mA. The chargeability was recorded in 9 time windows with increasing durations from 0.01 to 0.980 s after current turn-off.

We have used the gradient array combined with dipole measurements outside the current electrodes, in order to take full advantage of the number of measuring channels, and because the combination of these arrays has shown to provide good geometrical resolution (numerical modeling results, yet partly unpublished).

The lines are measured using the roll-along technique (Dahlin, 1993) which ensures field efficiency when measuring long lines. For each line and each day in the field, the measurements were repeated (or stacked) three times at the first station to control the repeatability. Thereafter they were only measured once in most cases to be able to finish the measurements in the limited available time (Figure 75).

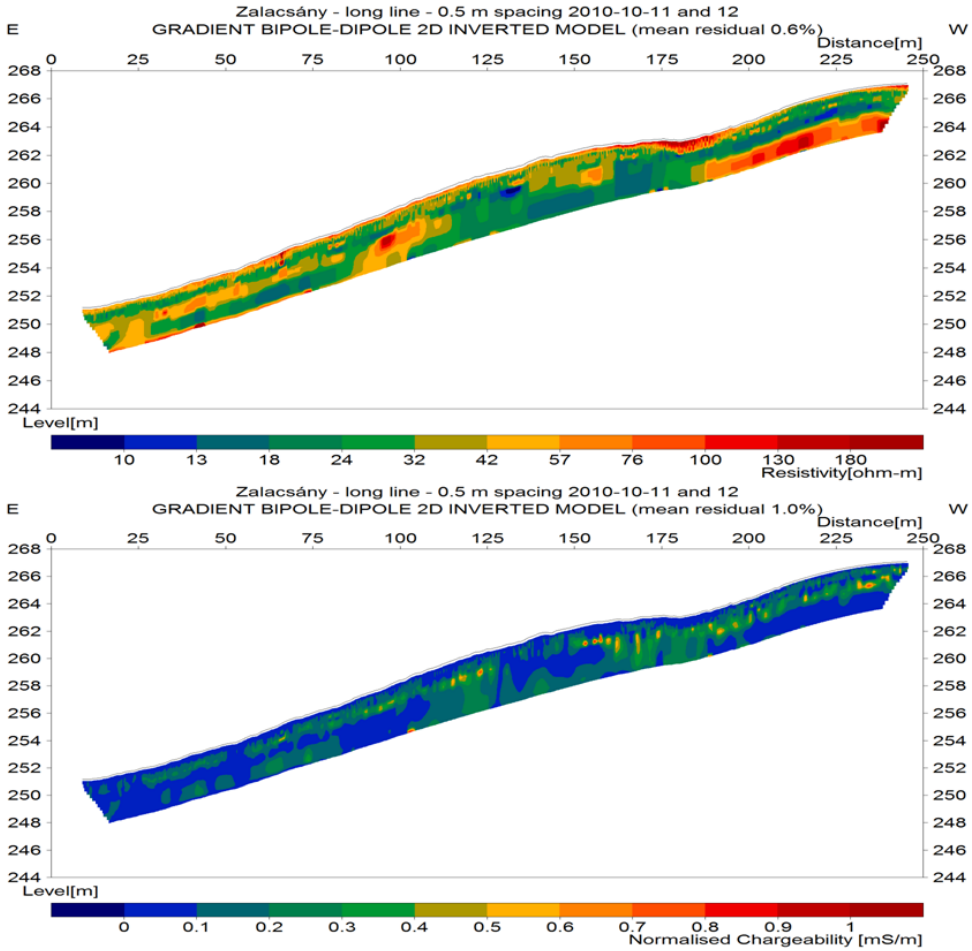

Figure 75 : Zala geoelectric profiles

The following table summarize the total experiment works :

Date	Lines measured	Number of measured points	Other tasks performed	Number of persons in the field
9th October	1:		Choice and marking of the line	2 (about 2x5 hours)
11th October	1:		Soil sampling (one disturbed soil sample every 10 m) Marking of the line	3 (about 3x 10 hours)
12th October	2:		Soil sampling (one disturbed soil sample every 10 m) Positioning with differential GPS Marking of the line	4 (about 2x5 hours + hours in the lab /about 2x 8 hours)

5. Conclusion

The present deliverable concerns the second task of the DIGISOIL's WP3. After Before their test in controlled conditions, the geophysical methods have been tested in real field conditions to produce soil properties maps. This report aims to present all these experiments and discusses the ability of geophysical methods to produce soil properties maps. These experiments will comfort the conversion step described in deliverable D2.2 – D2.3, i.e. the assimilation, correction steps realized on calibration sites.

Each experiment has been presented classified by each geophysical method: geoelectric, EMI and GPR, magnetism, hyperspectral and seismic. The soil variables of interest were water content, bulk density, clay content and organic carbon content. Variables used for correcting dataset were also obtained as soil stone content. Soil depth and thickness were also estimated, in particular, by seismic method.

6. References

Burgess, T.M., Webster, R. and McBratney, A.B., 1981. Optimal interpolation and isarithmic mapping of soil properties. 4 Sampling strategy. J Soi Sci., 32, 643-649.

Grandjean, G., Bitri, A., Cousin, I., Lambot, S., André, F., 2009. Description of processing protocols for each sensor. Report N°FP7-DIGISOIL-D1.2, 40 pages.

Kanlinowski, A. and Oliver, S., 2004. ASTER Mineral Index Processing. Remote Sensing Application Geoscience Australia. Australian Government Geoscience Website: http://www.ga.gov.au/image_cache/GA7833.pdf

Lambot, S., Slob, E.C., van den Bosch, I., Stockbroeckx, B., Vanclooster, M., 2004. Modeling of ground-penetrating radar for accurate characterization of subsurface electric properties. Ieee Transactions on Geoscience and Remote Sensing, 42(11): 2555-2568.

Lambot, S., André, F., Grandjean, G., Samyn, K., Van Wasemael, B., Stevens, A., Chiarantini L., Cousin I., 2009. Measuring and processing protocols description. Report N°BRGM/FP7-DIGISOIL-D1.3, 60 pages.

Lambot S., F. André, D. Moghadas, E.C. Slob, H. Vereecken, 2009. Analysis of full-waveform information content in ground penetrating radar and electromagnetic induction data for reconstructing multilayered media, Proceedings of the 2009 5th International Workshop on Advanced Ground Penetrating Radar, 5 pages, IWAGPR 2009, Grenada, Spain, 27-29 May 2009.

Moghadas, D., Andre, F., Slob, E.C., Vereecken, H. and Lambot, S., 2010. Data Fusion of Ground Penetrating Radar and Electromagnetic Induction for Reconstruction of Soil Electrical Properties. Near Surface 2010, 6 - 8 September 2010, Zurich, Switzerland.

Matheron, G., 1965. Les variables generalises et leur estimation. Masson, Paris.

Myers, D. E., 1994. Spatial interpolation: an overview. Geoderma 62, 17-28.

Rhoades, J.D., Raats, P.A.C., Prather, R.J., 1976. Effects of liquid-phase electrical conductivity, water content, and surface conductivity on bulk soil electrical conductivity. Soil Science Society of America Journal, 40(5): 651-655.

Sheets, K.R., Hendrickx, J.M.H., 1995. Noninvasive soil-water content measurement using electromagnetic induction. Water Resources Research, 31(10): 2401-2409.

Stevens, A., Udelhoven, T., Denis, A., Tychon, B.,, Lioy, R., Hoffmann, L. and Bas van Wesemael, 2010.vMeasuring soil organic carbon in croplands at regional scale using airborne imaging spectroscopy. Geoderma, 158, 1-2, 32-45.

Topp, G.C., Davis, J.L., Annan, A.P., 1980. Electromagnetic determination of soil water content: measurements in coaxial transmission lines. Water Resources Research, 16(3): 574-582.

Scientific and Technical Centre
RNSC Division
3, avenue Claude-Guillemin - BP 36009
45060 Orléans Cedex 2 – France – Tel.: +33 (0)2 38 64 34 34